Tracking along-arc sediment inputs to the Aleutian arc using thallium isotopes

Sune G. Nielsen[1,2*], Gene Yogodzinski[2], Julie Prytulak[3], Terry Plank[4], Suzanne M. Kay[5], Robert W. Kay[5], Jerzy Blusztajn[1,2], Jeremy D. Owens[1,2], Maureen Auro[1] and Tristan Kading[1]

[1]NIRVANA laboratories, Woods Hole Oceanographic Institution, Woods Hole, MA, USA
[2]Dept. of Geology and Geophysics, Woods Hole Oceanographic Institution, Woods Hole, MA, USA
[3]Department of Earth and Ocean Sciences, University of South Carolina, Columbia, SC, USA
[4]Department of Earth Science and Engineering, Imperial College London, UK
[5]Lamont Doherty Earth Observatory, Columbia University, NY, USA
[6]Department of Earth and Atmospheric Sciences, Cornell University, Ithaca, NY, USA

* corresponding author: snielsen@whoi.edu

Abstract - Sediment transport from the subducted slab to the mantle wedge is an important process in understanding the chemical and physical conditions of arc magma generation. The Aleutian arc offers an excellent opportunity to study sediment transport processes because the subducted sediment flux varies systematically along strike (Kelemen et al., 2003) and many lavas exhibit unambiguous signatures of sediment addition to the sub-arc mantle (Morris et al., 1990). However, the exact sediment contribution to Aleutian lavas and how these sediments are transported from the slab to the surface are still debated. Thallium (Tl) isotope ratios have great potential to distinguish sediment fluxes in subduction zones because pelagic sediments and low-temperature altered oceanic crust are highly enriched in Tl and display heavy and light Tl isotope compositions, respectively, compared with the upper mantle and continental crust.

Here, we investigate the Tl isotope composition of lavas covering almost the entire Aleutian arc a well as sediments outboard of both the eastern (DSDP Sites 178 and 183) and central (ODP Hole 886C) portions of the arc. Sediment Tl isotope compositions change systematically from lighter in the Eastern to heavier in the Central Aleutians reflecting a larger proportion of pelagic sediments when distal from the North American continent. Lavas in the Eastern and Central Aleutians mirror this systematic change to heavier Tl isotope compositions to the west, which shows that the subducted sediment composition is directly translated to the arc east of Kanaga Island. Moreover, quantitative mixing models of Tl and Pb, Sr and Nd isotopes reveal that bulk sediment transfer of ~0.6-1.0% by weight in the Eastern Aleutians and ~0.2-0.6% by weight in the Central Aleutians can account for all four isotope systems. Bulk mixing models, however, require that fractionation of trace element ratios like Ce/Pb, Cs/Tl, and Sr/Nd in the Central and Eastern Aleutians occurs after the sediment component was mixed with the mantle wedge. Models of Sr and Nd isotopes that involve sediment melting require either high degrees of

sediment melting (>50%), in which case trace element ratios like Ce/Pb, Cs/Tl, and Sr/Nd of Aleutian lavas need to be produced after mixing with the mantle, or significant fluid additions from the underlying oceanic crust with Sr and Nd isotope compositions indistinguishable from the mantle wedge as well as high Sr/Nd ratios similar to that of low (<20%) degree sediment melts.

Thallium isotope data from Western Aleutian lavas exhibit compositions slightly lighter than the upper mantle, which implies a negligible sediment flux at this location and probably involvement of low-temperature altered oceanic crust in the generation of these lavas. In general, the lightest Tl isotope compositions are observed for the highest Sr/Y ratios and most unradiogenic Sr and Pb isotope compositions, which is broadly consistent with derivation of these lavas via melting of eclogitized altered oceanic crust.

1. Introduction

Volcanic arcs are the surface expression of plate subduction, which controls the transfer of volatiles and other chemical heterogeneities into Earth's mantle. Subduction zones are also the centers of the most pronounced natural hazards on Earth due to their frequent volcanic eruptions as well as great earthquakes. It is therefore important to understand the physical and chemical mechanisms that are responsible for generating volcanic arcs.

Material erupted from arc volcanoes are derived from two principal sources: The subducting slab and the mantle wedge located between the slab and arc crust. While the mantle wedge often is considered to consist of relatively homogenous depleted peridotite, the subducting slab is highly heterogeneous, and it is uncertain which portions of it are released into the volcanic arc and which portions are ultimately subducted into the deep mantle (Ryan and Chauvel, 2014). The subducting slab contains sediments, variably altered oceanic crust (AOC), ultramafic cumulates and mantle rocks, some of which may be substantially hydrated. Uncertainties associated with determining mass fluxes from the slab make it difficult to construct models of the distribution and origin of chemical and physical heterogeneities in the deep Earth and thereby understanding mantle geodynamics and terrestrial volatile budgets.

Sediments are known to contribute to many arc lavas (Carpentier et al., 2008; Morris et al., 1990; Plank, 2005; Tera et al., 1986), but their exact fluxes from the slab are particularly difficult to quantify, in part because they likely represent a very small fraction of the material contained in arc lavas (Ben Othmann et al., 1989; Kay, 1980; Thirlwall et al., 1996; White and Dupré, 1986). Sediments may also be scraped off the slab into forearc accretionary complexes along some margins (Von Huene and Scholl, 1991). At the same time, sediments often contain very high concentrations of many trace elements compared with the mantle wedge (Ben Othmann et

al., 1989; Plank and Langmuir, 1998), which could enable detection of even minor sediment additions to arc lavas. However, many of these trace elements may be strongly affected by retention in accessory mineral phases that likely exist in the slab (Hermann and Rubatto, 2009; Johnson and Plank, 1999; Skora and Blundy, 2010), which further complicates the assessment of sediment contributions to volcanic arcs.

The Aleutian arc provides an excellent opportunity to study geochemical fluxes from slab to surface because previous studies have shown that subducted marine sediments unambiguously contribute to most Aleutian lavas (Kay and Kay, 1994; Morris et al., 1990; Plank, 2005; Sun, 1980; Tera et al., 1986). In addition, there is a systematic decrease in subduction rate from east to west while only relatively minor variations occur in the overall sediment thickness subducted along the main arc (e.g. Kelemen et al., 2003). Thus, the sediment subduction flux is thought to be highest in the east and almost absent in the westernmost portions of the arc (Kay and Kay, 1994). The question, however, is whether the sedimentary flux beneath the arc is also reflected in the magnitude of the sediment component in the arc volcanic rocks and, hence, if the fraction of sediment removed from the slab to the arc is independent of total sediment subduction flux. Several studies have also suggested that the chemical characteristics of the subducted sediment are likely to change along the arc from thick continental detrital in the east (turbidites of the Zodiac and Surveyor fans) to abyssal pelagic clays in the central Aleutians (Kay and Kay, 1988; Kay and Kay, 1994; Sun, 1980; Yogodzinski et al., 2010), which should be manifested in the isotopic characteristics of Aleutian lavas. However, this trait has yet to be confirmed, partially because no direct measurements of pelagic sediments outboard of the Central Aleutians have been conducted to date.

An additional interesting feature of the Aleutian arc is the presence of lavas that may reflect melting of eclogitized subducted oceanic crust due to their high silica, high Sr/Y, and unradiogenic Pb and Sr isotope compositions (Kay, 1978; Yogodzinski et al., 2015; Yogodzinski et al., 1995; Yogodzinski et al., 2001). These lavas are predominant in the Western part of the arc with Miocene-age examples from Adak Island (Kay, 1978) giving rise to the name of the rock type adakites (Defant and Drummond, 1990).

Here we use thallium (Tl) isotope ratios to assess sediment fluxes to the Aleutian arc. Thallium isotopes have great potential to quantify fluxes from the slab because modern pelagic sediments are highly enriched in Tl and display isotopic compositions that are heavier than the isotopically homogeneous upper mantle (Nielsen and Rehkämper, 2011; Prytulak et al., 2013; Rehkämper et al., 2004). Oceanic crust altered by hydrothermal fluids at low temperatures (<100°C), on the other hand, display light Tl isotope compositions coupled with high Tl concentrations (Coggon et al., 2014; Nielsen et al., 2006c). Therefore, the diversity of previously inferred source regions of the Aleutian arc provides an ideal setting to employ Tl isotopes as a slab component tracer.

2. Thallium isotope background

Thallium is a trace metal that displays both lithophile and chalcophile behaviors. In geochemical studies, it is often grouped with the alkali elements K, Rb, and Cs due to their similar ionic radii and charge (Heinrichs et al., 1980; Shannon, 1976; Shaw, 1952). However, a recent study found that Tl is compatible in mantle sulfides and therefore has a higher bulk partition coefficient during mantle melting than do the alkali metals (Nielsen et al., 2014). Nonetheless, Tl is incompatible during mantle melting and is enriched in the continental crust

(~300-500 ng/g) relative to the mantle (~0.5-2 ng/g) and mid ocean ridge basalts (~2-20 ng/g) (Nielsen et al., 2005; Nielsen et al., 2014; Wedepohl, 1995).

Thallium has two stable isotopes with masses 203 and 205. Thallium isotope compositions are reported relative to the NIST SRM 997 Tl standard in parts per 10,000 such that

$$\varepsilon^{205}Tl = 10{,}000 \times ({}^{205}Tl/{}^{203}Tl_{sample} - {}^{205}Tl/{}^{203}Tl_{SRM\ 997})/({}^{205}Tl/{}^{203}Tl_{SRM\ 997}) \quad (1)$$

It is thought that the small relative mass difference between the two isotopes prevents extensive isotopic fractionation in all but a select few environments, which may be linked to nuclear volume isotope fractionation that occurs in chemical reactions primarily involving both oxidation states of Tl, +1 and +3 (Nielsen and Rehkämper, 2011; Schauble, 2007). Trivalent Tl, however, is not likely to be thermodynamically stable in the igneous environments including the mantle given that Tl dissolved in oxic seawater is exclusively univalent (Byrne, 2002; Nielsen et al., 2009). The univalent Tl redox state of the mantle renders the average upper mantle homogenous with respect to Tl isotopes ($\varepsilon^{205}Tl_{MORB} = -2 \pm 0.5$; (Nielsen et al., 2006b)) because no significant isotope fractionation is expected during melting or fractional crystallization (Schauble, 2007). In contrast, hydrothermally altered oceanic crust and metalliferous marine sediments are highly variable with respect to Tl isotope ratios and concentrations.

Enrichment of Tl in marine sediments is primarily due to adsorption onto authigenic manganese (Mn) oxides (Hein et al., 2000; Nielsen et al., 2013; Rehkämper et al., 2004; Rehkämper et al., 2002) that precipitate ubiquitously from oxic seawater onto sedimentary particles. This adsorption process is responsible for heavy Tl isotope compositions detected in pelagic clays of $\varepsilon^{205}Tl > 2$ (Rehkämper et al., 2004) and is probably linked to surface oxidation of Tl during adsorption to Mn oxides (Nielsen et al., 2013; Peacock and Moon, 2012). Rates of Mn oxide precipitation are very slow, thus the abundance of Mn oxides in sediments generally

150 inversely correlates with sediment depositional rates. This process renders sediments deposited
151 close to continents or underneath highly productive water masses depleted in Tl associated with
152 Mn oxides and consequently such sediments are characterized by ε^{205}Tl ~ -2, akin to the
153 continental crust and the upper mantle (Nielsen et al., 2006b; Nielsen et al., 2005; Nielsen et al.,
154 2006c).

155 In the basaltic oceanic crust, Tl enrichment occurs within the upper few hundred meters of
156 the oceanic crust during the circulation of seawater at low temperatures (<100°C). Thallium
157 enrichment may be related to biologically mediated pyrite precipitation (Coggon et al., 2014) or
158 alternatively to Tl partitioning into alkali-rich clay minerals that also form during low
159 temperature alteration (Nielsen et al., 2006c). Analysis of Tl concentrations and isotope
160 compositions in low-T altered crust from IODP Hole U1301B, Deep Sea Drilling Project
161 (DSDP) Hole 417D and DSDP/Ocean Drilling Project (ODP) Hole 504B showed high Tl
162 concentrations (30-1000 ng/g) and light Tl isotope ratios (down to ε^{205}Tl ~ -15; (Coggon et al.,
163 2014; Nielsen et al., 2006c)). Conversely, the sheeted dike portion of the oceanic crust is
164 depleted in Tl (<1 ng/g; (Nielsen et al., 2006c)), which is the result of hydrothermal fluid
165 circulation at high temperature (300-400°C) near the ridge axis that drives extraction rather than
166 deposition of Tl. This process does not appear to cause isotope fractionation, however, as sheeted
167 dikes have ε^{205}Tl similar to MORB glass (ε^{205}Tl ~ -2 ± 0.5; (Nielsen et al., 2006b; Nielsen et al.,
168 2006c)).

169 The Tl isotope systematics of marine sediments and oceanic crust combined with previous
170 studies of the Aleutian arc allow some general predictions to be made about what Tl isotope
171 compositions to expect in different portions of the Aleutian arc. Sediment fluxes from the slab
172 have been inferred to account for the majority of the observed trace element and isotopic

enrichments in the eastern and central portions of the arc (Kay et al., 1978; Kelemen et al., 2003; Yogodzinski et al., 2010). The turbidites of the Surveyor and Zodiac fans (Fig, 1) supply primarily detrital sediments to the eastern portion of the arc, while the Central Aleutians are sufficiently distal to any continent that slowly accumulating pelagic clays become the dominant sediment type in that region. Given that Tl isotope compositions of detrital sediments (ε^{205}Tl ~ -2) and pelagic clays (ε^{205}Tl > 0) are distinct, we might expect the Central Aleutians to display somewhat heavier Tl isotope compositions than do the Eastern Aleutians. The Western Aleutians, on the other hand, are often inferred to have almost negligible sediment input. Instead, adakitic lavas that may be derived from melting of the down-going oceanic crust are common (Yogodzinski et al., 2015; Yogodzinski et al., 2001). If the upper volcanic portion of the oceanic crust that has previously been hydrothermally altered at low temperatures takes part in these melting processes, then Tl isotope compositions of ε^{205}Tl < -2 are expected.

3. Samples

3.1. Aleutian lavas

Lava samples from the east and central Aleutians (from Okmok, Westdahl, Moffett and Kanaga volcanoes) were originally chosen to explore Th-Nb-REE variations with high quality ICP-MS analyses, and are the same as those published and discussed in Plank (2005) and Kay and Kay (1994). This subset of Aleutian volcanic rocks form a tight linear trend in Th/La-Sm/La that were interpreted to derive from simple binary mixing between mantle and a sedimentary component that is nearly identical to the DSDP 183 sediment average. These samples thus show clear evidence for subducting sediment in their source, largely of continental detrital (high Th/La) origin**.**

Western Aleutian samples were dredged from locations west of Buldir Volcano, which is the westernmost emergent volcano in the Aleutian arc (Fig. 1). The samples are from volcanic cones of the Ingenstrem Depression, a rectangular-shaped structural depression immediately west of Buldir, and from the Western Cones area, which is located 200-300 km further west. Ages of the samples are uncertain, but all were dredged from constructional volcanic edifices which, based on available dating, appear to be no more than 500-600 ka years old (Yogodzinski et al., 2015). Petrographic observations indicate that the samples are fresh and apparently unaffected by weathering or other alteration processes. Additional details, including geochemical methods, complete whole-rock compositions, petrographic descriptions and photomicrographs are provided in Yogodzinski et al. (2015).

3.2. Sediment samples

Thallium isotope compositions and concentrations were determined for discrete sediment samples from Deep Sea Drilling Program (DSDP) Sites 178 and 183 and Ocean Drilling Program (ODP) Hole 886C (Fig. 1).

Sites 178 and 183 are both located outboard of the eastern portion of the Aleutian arc with DSDP Site 178 located in the Gulf of Alaska and therefore slightly to the east of the Aleutian islands, but representative of sediments of the Surveyor Fan. The samples analyzed here from DSDP 178 have previously been investigated for both trace elements and some radiogenic isotope ratios (Plank and Langmuir, 1998; Vervoort et al., 2011). Samples from DSDP 183 are new samples that were obtained from core depths adjacent (2cm) to the samples that had previously been used to assess the composition of subducted sediment in the Aleutians (Kay and Kay, 1988; Plank and Langmuir, 1998; Vervoort et al., 2011; Von Drach et al., 1986).

Sediment samples from ODP Hole 886C were also obtained, which is located outboard of the Central Aleutians on the abyssal plain at 44°41.384'N, 168°14.416'W. The sediment thickness in this location is ~70m with an estimated maximum age of ~80Ma (Snoeckx et al., 1995). However, the upper ~50m were deposited in the last 10 million years while the bottom ~20m are characterized by several hiatuses and very slow deposition rates (Snoeckx et al., 1995). We selected 15 samples at approximately evenly distributed intervals (Table 1). Each sample was selected by visual inspection of core barrels in order to obtain the most representative samples from each section. The types of sediment analyzed range from diatom ooze to dark brown pelagic clay. Several ferromanganese (Fe-Mn) nodules are also found in Hole 886C and because such nodules often contain large enrichments of many trace metals we also selected one of these here (886C 6H-3 120-122cm) to assess the effect on the trace element budget in the average subducted sediment composition. A single sample from the uppermost altered basaltic basement at Site 886B (Table 1) was also obtained in order to potentially assess the composition of the hydrothermally altered basaltic crust in the Central Aleutians.

4. Methods

4.1. Sample preparation and chemical separation of Tl, Sr, Nd and Pb

The eastern and central Aleutian lavas were powdered as part of the study in Kay and Kay (1994) and Plank (2005) in an alumina ball mill to eliminate Nb-Ta contamination in samples previously powdered in tungsten carbide. Sediment samples from ODP Hole 886C were dried in an oven at 80°C overnight before powdering in an agate swing mill. The swing mill was cleaned with high purity quartz before and after each run, triple rinsed with deionized water and air dried to avoid cross-contamination. Lavas from the Western Aleutians consist of submarine dredges

primarily from the Ingenstrom depression (~ 52°30'N, 175°W) were obtained as rock fragments of ~50g. Due to potential alteration by interaction with seawater and possible contamination with Fe-Mn minerals precipitated from seawater, we did not powder these samples. Instead each sample was fractured into mm-sized chips. These were handpicked under a binocular microscope to select pieces devoid of alteration and Fe-Mn minerals. The rock chips were then ultrasonicated in MQ water to remove any dust or superficial contaminants. Additional tests were also performed on a subset of the Western Aleutian lavas in order to investigate if alteration or Fe-Mn minerals were present in the otherwise visually pure rock chips. These tests involved separating three additional aliquots of rock chips. These three splits were 1) dissolved without further preparation, 2) ultrasonicated for 1 hour in 1M distilled HCl prior to dissolution and 3) ultrasonicated for one hour in 6M distilled HCl prior to dissolution. For two of the 1M HCl leachates sufficient Tl was present for Tl isotope analysis.

Chips as well as powdered samples (0.1-0.3g) were dissolved in a 1:1 mixture of concentrated distilled HF and HNO_3 on a hotplate overnight. Following this, they were dried and fluxed several times with concentrated distilled nitric acid and hydrochloric acid until the fluorides that formed during the first step could no longer be seen. Separate powder splits of the Central Aleutian lavas were dissolved for Tl, Sr, Nd and Pb isotopes. Following complete dissolution of fluorides, samples were dried on a hotplate and taken up in appropriate acid matrices for separation of Tl, Sr, Nd and Pb, respectively. Isolation of Tl, Sr, Nd and Pb from sample matrix followed previously published ion exchange chromatographic methods (Baker et al., 2009; Jackson and Hart, 2006; Lugmair and Galer, 1992; Nielsen et al., 2004; Rehkämper and Halliday, 1999; Scher and Delaney, 2010). Strontium was separated and purified from samples using Sr-Spec (Eichrom® Technologies, Inc.) resin. Neodymium chemistry was done

265 with LN resin (Eichrom® Technologies, Inc.) following methods described in Scher and Delaney
266 (2010). Lead chemistry utilized the HBr-HNO_3 procedure of Lugmair and Galer (1992) and
267 Abuchami et al. (1999). The Tl separation procedure has been shown to produce quantitative
268 yields (Nielsen et al., 2004; Nielsen et al., 2006a; Rehkämper et al., 2004) and these can
269 therefore be converted to Tl concentrations. Total procedural Tl blanks during this study were
270 <3pg, which is insignificant compared to the indigenous Tl processed for the samples of >3ng.
271 Total chemistry blanks for Sr, Nd and Pb were 60pg, 5pg and 50pg, respectively, which is
272 significantly less than the minimum amounts processed of 15µg, 1µg, and 200ng, respectively.
273
274 ***4.2. Determination of Tl isotope compositions and concentrations***
275 The Tl isotope compositions were determined at the WHOI Plasma Mass Spectrometry
276 Facility using a Thermo Finnigan Neptune multiple collector inductively coupled plasma-mass
277 spectrometer (MC-ICPMS). Previously described techniques that utilize both external
278 normalization to NIST SRM 981 Pb and standard-sample bracketing were applied for mass bias
279 correction (Nielsen et al., 2004; Rehkämper and Halliday, 1999). Due to the quantitative yields
280 of Tl from the column chemistry procedure, Tl concentrations were determined by monitoring
281 the ^{205}Tl signal intensities of the samples during the isotopic measurements. A known quantity of
282 NIST SRM 981 Pb was added to the sample Tl and the measured ^{205}Tl/^{208}Pb ratios were then
283 converted directly into Tl abundances. Previous studies (Nielsen et al., 2007; Nielsen et al.,
284 2006b; Nielsen et al., 2006c) that utilized the Nu Plasma MC-ICPMS applied a 5% correction
285 that assumed Tl ionises 5% more efficiently than Pb. However, we have not been able to verify
286 this behavior for the Neptune and thus do not apply this correction here. The uncertainty on the
287 Tl concentration measurements is likely on the order of ±10% (2sd) (Prytulak et al., 2013).

During the course of this study we evaluated the external Tl isotope reproducibility with repeat analyses of USGS reference basalt powder BHVO-1, which was found to have an isotope composition of ε^{205}Tl = -3.5 ± 0.5 (2sd) (Nielsen et al., 2015). Although individual Tl isotope analyses have internal counting statistical uncertainties of about 0.07-0.15 ε^{205}Tl-units (1se), we apply the external 2sd reproducibility of 0.5 ε^{205}Tl-units to all unknowns because this uncertainty accounts for all possible sources of error including sample dissolution, ion exchange chromatography and mass spectrometric procedures (Nielsen et al., 2004).

4.3. Determination of Sr, Nd and Pb isotope compositions

Strontium, Nd and Pb isotopic measurements were performed on a Thermo Finnigan Neptune MC-ICPMS at the WHOI Plasma Mass Spectrometry Facility. For Sr isotope measurements, isobaric interferences of ^{87}Rb on ^{87}Sr and ^{86}Kr on ^{86}Sr were corrected for by monitoring ^{82}Kr, ^{83}Kr and ^{85}Rb. Mass bias was corrected for with the exponential mass fractionation law assuming ^{86}Sr/^{88}Sr = 0.1194, with a secondary correction to the Sr standard NIST SRM 987 (^{87}Sr/^{86}Sr=0.710214) (Jackson and Hart, 2006). These secondary corrections were always smaller than 40 ppm. The internal precision for Sr isotopic measurements was 8-14 ppm (2se), while repeat measurements of the NIST SRM 987 standard yielded external precision of ~25 ppm (2se).

For Nd isotope measurements, ^{147}Sm and ^{149}Sm were monitored to correct for the ^{144}Sm interference on ^{144}Nd. The interference corrected Nd isotope data were internally corrected for mass bias using the exponential mass bias law, assuming ^{146}Nd/^{144}Nd = 0.7219, with a secondary correction to JNdi-1 (^{143}Nd/^{144}Nd=0.512104, (Tanaka et al., 2000)). These secondary corrections

were always smaller than 20 ppm. The internal precision of individual analyses was 8-12 ppm (2se) and the external precision, assessed through repeat analyses of JNdi-1, was ~15 ppm (2se).

Lead isotope compositions were externally normalized for instrumental mass bias relative to $^{205}Tl/^{203}Tl$ = 2.3871 for the NIST SRM 997 Tl standard and were also corrected using measurements of NIST SRM 981 using values from Todt et al. (1996). The Pb isotopic ratios have internal precision of 15-60 ppm for $^{206}Pb/^{204}Pb$, $^{207}Pb/^{204}Pb$, and $^{208}Pb/^{204}Pb$. External reproducibility was assessed through repeat measurements of NIST SRM 981 and range from 17 ppm (2se) for $^{207}Pb/^{206}Pb$ to 120 ppm (2se) for $^{208}Pb/^{204}Pb$.

The well-characterized USGS rock standard BHVO-1 was dissolved, processed, and analyzed along with unknowns. Results for Pb, Sr and Nd isotopic measurements of the BHVO-1 rock standard (Table S1) are within error of those reported in Weis et al. (Weis et al., 2006; 2005).

4.4. Trace element concentration analyses

The Eastern and Central Aleutian lavas were digested and analyzed by ICP-MS, as described and given in Plank (2005). DSDP 183 and 178 sediments were analyzed by INAA, DCP and ICP-MS sediments as described and presented in Kay and Kay (1988), Plank and Langmuir (1998) and Vervoort et al (2011), respectively. The ODP 886C sediments were analyzed by ICP-MS and ICP-ES at Lamont-Doherty Earth Observatory as part of this study, following procedures described in Rabinowitz et al (2015). Calibration standards and data quality are as reported in Rabinowitz et al. (2015). Notably, thallium concentrations were determined to within 3% relative standard deviation based on three separate digestions of the Indian Ocean Radiolarian Clay (407 ± 11 ng/g).

5. Results

Thallium isotopic variation in the Eastern and Central Aleutian Islands (Unimak to Kanaga, Fig. 1) ranges from $\varepsilon^{205}Tl$ = -3.8 to +2.6 (Table 2). The vast majority of samples, however, have values that are within error of or heavier than the average upper mantle and continental crust ($\varepsilon^{205}Tl$ = -2). The largest spread in Tl isotope compositions are found in samples from Adak and Kanaga islands whereas samples in the eastern Aleutians tend to cluster around the value for average upper mantle and continental crust ($\varepsilon^{205}Tl$ = -2). Samples in this study from Adak and Kanaga islands also cover the largest range in age (Kay and Kay, 1994), which may partially account for the larger Tl isotope diversity. For the most mafic lavas (SiO_2 <54%), Tl concentrations range between 25 and 97 ng/g, which is significantly enriched compared to 2-20 ng/g observed for most MORB (Jenner and O'Neill, 2012; Nielsen et al., 2014).

Lavas from the Western Aleutians are characterized by lighter Tl isotope compositions than the Central and Eastern Aleutians with most samples exhibiting $\varepsilon^{205}Tl$ = -3.4 to -1.5. Two samples have somewhat heavier Tl isotope compositions close to $\varepsilon^{205}Tl$ = 0 while one sample is very light at $\varepsilon^{205}Tl$ = -9.3 (Table 3). Thallium concentrations in the Western Aleutian lavas overlap with those recorded for basaltic samples from the Eastern and Central Aleutians, but also extends up to 470 ng/g for the very light sample. It is important to note that repeat analyses of Western Aleutian lavas often showed a range of concentrations (Table 3). Some of this variation can possibly be ascribed to the presence of contamination from Fe-Mn minerals or alteration via interaction with seawater. However, a large fraction of this variation is clearly unrelated to these secondary processes as the four different analyses of sample TN182_07_002 varies by more than a factor of five (Table 3). The most likely explanation for the large concentration differences is

that the Western Aleutian rocks are crystalline with a mixture of mineral grains up to several mm in diameter and groundmass (Yogodzinski et al., 2015). Each Tl isotope analysis was performed on separately handpicked rock chips, not from a homogenized rock powder. Most igneous minerals (olivine, pyroxene, plagioclase, amphibole) likely contain very low Tl concentrations (Adam and Green, 2006) and, hence, it is expected that samples are heterogeneous on the mm-scale with respect to Tl concentrations. With this caveat in mind, we emphasize that element ratios involving Tl for Western Aleutian samples likely have uncertainties that approach a factor of two. All other Tl isotope analyses were performed on homogenous rock powders and are therefore not prone to effects of heterogeneity.

Sediments outboard of the Aleutian arc display Tl isotope compositions from $\varepsilon^{205}Tl$ = -3.1 to +10.9 (Table 4), while Tl concentrations also vary strongly between 55 to ~20000 ng/g. Although most samples fall in the range from $\varepsilon^{205}Tl$ = -3 to -1, there is a clear tendency for the most Tl –rich samples to display the heaviest Tl isotope compositions (Fig. 2). In addition, it is evident that samples from ODP Site 886C exhibit, on average, heavier Tl isotope compositions and higher Tl concentrations than do the sediments from DSDP 178 and 183 (Fig. 2), which is clearly related to the high abundance of Fe-Mn minerals in certain sections of ODP Site 886C sediments. Another striking feature of the pelagic sediments from ODP Site 886C outboard of the Central Aleutians is that $^{206}Pb/^{204}Pb$ and $^{208}Pb/^{204}Pb$ isotope compositions of many samples are significantly less radiogenic than those found in DSDP Holes 178 and 183 that are further to the east (Table 4). This effect is likely due to the presence of Pb-rich Fe-Mn minerals that precipitate directly from North Pacific seawater, which is thought to have been unradiogenic throughout the Cenozoic (Ling et al., 1997; Ling et al., 2005). In addition, the oldest and most Pb-enriched pelagic sediments in Hole 886C also display very unradiogenic $^{207}Pb/^{204}Pb$, which

could indicate Pb inputs to seawater from MORB hydrothermal sources at this location. However, due to the large uncertainties on the sediment ages in the lower portion of ODP Hole 886C (Snoeckx et al., 1995) it is difficult to assess to what extent these sediments contain sufficient Pb to significantly affect the bulk subducted sediment $^{207}Pb/^{204}Pb$ isotope composition.

Here we use the trace element concentrations and isotope compositions determined for sediments outboard of the Aleutian Islands to construct weighted average subducted sediment compositions for the eastern and central Aleutians (Table 5). The averages were also weighted by lithological abundance and density (Table 1), which was determined based on sediment descriptions and core barrel photographs (Rea et al., 1993). It is assumed that the sediment pile found at ODP Hole 886C is similar to what has been subducted in the Central Aleutians for the past at least 10 Ma. This assumption is reasonable because the sediment depositional environments as a function of distance from the Aleutian arc in the direction of the plate motion have likely remained relatively constant over this time period. That is, the North Pacific is characterized by relatively high productivity resulting in diatom rich sediments whereas the Central Pacific gyres display low productivity and, therefore, are dominated by abyssal red clays. Below we use the average subducted sediment components to investigate how changing sediment composition along the Aleutian arc affects the composition of erupted lavas.

6. Discussion

6.1. Thallium isotopic variation induced by secondary processes

The Tl isotope compositions and concentrations recorded in volcanic rocks can be modified by a number of syn- and post-eruption processes such as degassing, subaerial aqueous alteration, submarine hydrothermal alteration and submarine precipitation of Fe-Mn minerals on sample

surfaces. In addition, assimilation of wall rock and fractional crystallization prior to eruption could also alter the Tl budget of the original magma if the Tl concentrations and/or isotope compositions of wall rock and crystallizing phases were different from that of the original magma. In the following sections we discuss the potential for these processes to have affected our Tl isotopic data for lavas from the Aleutian arc in order to assess how much Tl isotope variation can be directly linked to inputs from the subducted slab.

6.1.1. Submarine contamination and alteration of Western Aleutian samples

Lavas erupted under submarine conditions are easily contaminated with Tl either associated with clay minerals that form during alteration of the lava (Jochum and Verma, 1996) or due to precipitation of Fe-Mn oxyhydroxides that form ubiquitously in oxic seawater (Nielsen and Rehkämper, 2011). As outlined in section 2, both these components are characterized by very strong Tl enrichments compared with those found in mantle derived melts as well as substantial Tl isotope fractionation (Coggon et al., 2014; Nielsen et al., 2006c; Rehkämper et al., 2004). Thus, even minute amounts of these contaminants may completely alter the Tl concentration and isotope composition of a given sample. In order to eliminate these sources of contamination, we analyzed only rock chips of dredge samples (not powders), which were prepared as described above to eliminate possible effects of seawater-rock interaction. The results of these analyses reveal Tl isotope and concentration patterns for a few samples that could reflect alteration or Fe-Mn mineral contamination. Additional tests were, therefore, conducted on a subset of the samples to further investigate if contamination was significant (Table 3). These tests involved leaching two separate aliquots of chips in 1M HCl and 6M HCl, respectively, during ultrasonication. The results of these tests confirm that one sample (TN182_07_002) had clearly

425 been affected by minor Fe-Mn mineral contamination. This assessment was confirmed by
426 analysis of both an untreated aliquot of the sample as well as the 1M HCl leachate, both of which
427 showed heavy Tl isotope compositions as would be expected for Fe-Mn minerals (Nielsen et al.,
428 2013; Peacock and Moon, 2012; Rehkämper et al., 2002). It is notable that even though the 1M
429 HCl leachate contained only very small amounts of Tl (2 ng per gram of sample) the exceedingly
430 heavy Tl isotope composition of the leachate (ε^{205}Tl = +9.8), which is consistent with values
431 found in Fe-Mn crusts (Nielsen et al., 2011; Nielsen et al., 2009; Rehkämper et al., 2002),
432 approximately accounts for the small isotopic shift observed in the unleached samples. The
433 uncontaminated Tl isotope composition of the sample is, therefore, best represented by the
434 leached aliquots both of which display identical values of ε^{205}Tl = -1.8. We are confident that the
435 leaching process has not induced notable Tl loss or isotope fractionation in sample
436 TN182_07_002 because leaching of an uncontaminated sample (TN182_07_009) yielded a result
437 identical to the untreated sample aliquot (Table 3).
438
439 *6.1.2. Degassing*
440 Degassing should be expressed as a loss of Tl potentially associated with kinetic isotope
441 fractionation whereby the light Tl isotope would preferentially be lost. Thallium isotope
442 measurements of volcanic fumaroles did not find any systematic enrichment in ^{203}Tl (Baker et
443 al., 2009), suggesting that kinetic Tl isotope fractionation during degassing might be limited.
444 However, these effects have never been investigated for actual rocks, which makes it difficult to
445 predict the magnitude of Tl isotope and concentration effects from degassing.
446 Given that Tl partitioning during mantle melting is similar to that of Ce (Nielsen et al.,
447 2014), it could be inferred that unusually high Ce/Tl ratios coupled with heavy Tl isotope

compositions might be indicative of significant degassing. However, because Ce/Tl in both sediments and AOC (Ce/Tl ~ 100-400) is much lower than the upper mantle (Ce/Tl ~1100, (Nielsen et al., 2014)) variations in Ce/Tl are not necessarily due to degassing unless Ce/Tl significantly exceeds the mantle value. Except for three samples, all Aleutian lavas display Ce/Tl ratios significantly lower than the upper mantle (Fig. 3). In addition all samples fall within the field expected for mixing between the mantle and sediments or AOC (Fig. 3), which suggests that degassing did not significantly affect Tl concentrations or isotopes in the majority of the samples studied here.

Of the three samples that display significantly higher Ce/Tl than sediments and AOC, one (SAR-17) displays Ce/Tl and ε^{205}Tl within error of the upper mantle, which could be consistent with a melt largely unmodified by addition of slab material. However, Pb isotope ratios in SAR-17 and other samples from this volcano are much more radiogenic (Table 2) than the depleted MORB mantle (Workman and Hart, 2005), which likely reflects the influence of terrigenous sediments (Kay et al., 1978). Alternatively, the low Tl content of this sample may reflect degassing from a lava that either 1) had a starting Tl isotope composition significantly lighter than the normal mantle or 2) did not register any significant Tl isotope fractionation during degassing. The latter interpretation would be consistent with the data of Baker et al. (2009), which showed no systematic enrichment in ^{203}Tl for volcanic fumaroles.

The second sample (TN182_07_005) with Ce/Tl similar to the upper mantle is characterized by ε^{205}Tl significantly heavier than the upper mantle (Table 3), which is consistent with degassing coupled with kinetic Tl isotope fractionation. This conclusion is supported by the chemical compositions of samples TN182_07_009 and TN182_07_005, which were collected in close proximity to one another, being almost identical for all elements except Tl concentrations

and isotopes. It is unclear exactly why Tl isotopes are significantly different for these two samples, but, given the anomalous Tl isotope composition, we infer that TN182_07_005 was likely degassed and does not reflect the primary Tl isotope systematics of the original lava. Therefore, we will not consider it further in our discussion of slab-mantle interactions in the Aleutian arc and it has not been included in any figure except Figure 2.

The last sample to display Ce/Tl higher than the upper mantle is the Miocene adakite lava from Mt. Moffett (ADK53), which could indicate significant Tl degassing. However, the Tl isotope composition of ADK53 is not enriched in ^{205}Tl (Table 2), as might be expected from kinetic isotope fractionation. In addition, this sample has, based on its high Sr/Y and unradiogenic Sr and Pb isotope ratios, been proposed as a possible melt derived from eclogitized oceanic crust (Kay, 1978). Bulk Tl and Ce partition coefficients during melting of eclogite are unlikely to be identical to those found for mantle melting and therefore it is possible that Ce/Tl could be significantly altered during eclogite melting. Thallium partitions into sulfide (Kiseeva and Wood, 2013; Nielsen et al., 2014) and probably phengite (Prytulak et al., 2013) while Ce may be accommodated by allanite and/or epidote (Carter et al., 2015; Hermann, 2002). The relative abundances of these minerals will have a strong control on melt Ce/Tl especially at low degrees of melting where these phases potentially could be in the residue. However, given the lack of experimental data on Tl partitioning at relevant conditions it is currently not possible to constrain the effect on Ce/Tl during eclogite melting. Therefore, it we cannot conclusively distinguish between degassing or source mineralogy as the cause of the high Ce/Tl observed in ADK53.

For the remaining samples in this study we do not find any chemical or isotopic indications of significant degassing. If Tl degassing played a role in the Tl budgets of the lavas investigated

here, then the effects are too small to quantify and most likely smaller than the Tl elemental and isotopic signatures imposed by addition of subduction components.

6.1.3. Subaerial aqueous alteration

Subaerial lavas are often observed to preferentially lose alkali metals during aqueous alteration from meteoric water (Schiano et al., 1993). This effect is most likely due to the high solubility of these metals in aqueous solution and given the geochemical similarity between Tl and the alkali metals (i.e. ionic charge and radius as well as high aqueous solubility) one might expect subaerial alteration to be accompanied by significant Tl losses that would lead to high Ce/Tl ratios. These losses, however, would likely not be associated with Tl isotope fractionation because weathering has been shown to cause negligible Tl isotope fractionation (Nielsen et al., 2005).

High Ce/Tl ratios produced by subaerial weathering should be coupled with significant losses of alkali metals. Here we investigate this using Th/Rb as these two elements partition similarly in igneous processes while Th is highly insoluble in aqueous solution. Thus, high Th/Rb coupled with high Ce/Tl might indicate subaerial alteration. Figure 4 shows that only sample ADK53 has a clear signature that could be interpreted as subaerial alteration. Some alteration of ADK53 is also reasonable given that it is Miocene in age. All other samples investigated here are relatively recent, fresh lava flows that are unlikely to have experienced significant alteration. It should be noted that, while the trace element systematics of mobile elements like K, Rb, Cs and Tl may have been perturbed in ADK53, there is no indication that the original isotope compositions (radiogenic or Tl) of this lava have been reset by post-eruption

processes. We, therefore, use the isotopic characteristics of ADK53 in our discussion of subduction processes in the Aleutian arc, but omit trace element ratios from consideration.

6.1.4. Assimilation and fractional crystallization

Fractional crystallization in itself is not likely to alter the Tl isotope composition of magma. First, Tl is likely very incompatible in the major crystallizing phases like olivine, clinopyroxene and plagioclase (Adam and Green, 2006; Nielsen et al., 2014). Second, lavas from Korovin volcano (Atka Island) also support the lack of Tl isotope fractionation with magmatic differentiation. These Korovin lavas display patterns broadly consistent with evolution by fractional crystallization from basalt to high-silica andesite (Fig 5). Thallium is enriched in the more evolved lavas and the progressive Tl enrichment is not accompanied by any systematic Tl isotope change (Table 2), which confirms that fractional crystallization does not impart any detectable Tl isotope fractionation. The constancy of Tl isotopes for the more evolved samples also shows that any assimilation that might have occurred during fractional crystallization of the Korovin samples did not cause a notable change in Tl isotopes.

Even though fractional crystallization and assimilation appears to have a limited effect on Tl isotopes, we still choose to exclude samples from the Eastern and Central Aleutian Islands that bear evidence of magmatic evolution (>55 wt% SiO_2, <3% MgO and Mg# < 45) in order to remove any doubt that some Tl isotope variation could be caused by these processes. This step removes the three most evolved Korovin samples from consideration as well as one from Westdahl (SAR-4). It should be noted that all of the excluded samples display $\varepsilon^{205}Tl \sim -2$ (Table 2), which could indicate that assimilation of the arc crust tends to add Tl with an isotope

composition that is similar to continental crust. Hence, assimilation may possibly attenuate the Tl isotope variation of arc lavas.

One sample from the Western Aleutians (TN182_08_003) is unusually enriched in Tl compared with all other Aleutian samples (subaerial or submarine) investigated here. The sample displays Ce/Tl ~ 35, a factor of about 4 lower than any other sample in this study. It also has the lightest Tl isotope composition measured for the Aleutians (ε^{205}Tl = -9.3) and the leaching experiments confirmed that this value was unlikely to be caused by seawater alteration (Table 3). Inspection of the sample in thin section did not reveal any alteration minerals. However, the sample contains abundant amphibole phenocrysts many of which have resorbed textures indicating that amphibole was first crystallized and then started re-dissolving back into the melt (Yogodzinski et al., 2015). TN182_08_003 is the only basalt sample recovered from the Western Aleutians, which exhibits this texture, which may indicate that the liquid line of decent was interrupted potentially by assimilation of wall rock. If the magma chamber that hosted the lava prior to eruption was relatively shallow in the upper few km of the crust then the wall rock could be composed of low-temperature altered volcanic rocks, which are known to carry high Tl concentrations and very light Tl isotope compositions (Coggon et al., 2014; Nielsen et al., 2006c). Such assimilation processes would likely not affect radiogenic isotope systems like Pb, Nd and Sr because low-temperature AOC is not significantly enriched in these elements compared with fresh basalt and does not possess radiogenic isotope compositions that deviate substantially from fresh MORB and thereby also the compositions of the primary magma. Strontium isotope ratios of basaltic oceanic crust do become more radiogenic when interacting with seawater, but the vast majority of Sr isotope data for AOC in the literature display $^{87}Sr/^{86}Sr$ ~ 0.703-0.705 (Staudigel et al., 1995; Teagle et al., 2003), which is only slightly different to

TN182_08_003 that exhibits $^{87}Sr/^{86}Sr$ = 0.7033. We, therefore, conclude that this sample has been contaminated by assimilation of low-temperature AOC at relatively shallow crustal depths prior to eruption and do not consider it further in our discussion of Aleutian sub-arc mantle processes.

6.2. Sediment controls Tl isotope variation in the Central and Eastern Aleutian Islands

Excluding the sample that shows evidence of degassing (SAR-17) as well as the more evolved lavas (SAR-4, and three Korovin lavas) does not change the range of Tl isotope compositions recorded in the Eastern and Central Aleutian samples ($\varepsilon^{205}Tl$ = -3.8 to +2.6). We interpret these data as representative of the Tl isotope variation in the mantle sources of the Aleutian lavas investigated here. Only one sample (Kanaga S489, $\varepsilon^{205}Tl$ = -3.8) is lighter than the normal mantle value of $\varepsilon^{205}Tl = -2 \pm 0.5$ (Nielsen et al., 2007; Nielsen et al., 2006b; Nielsen et al., 2006c) with 13 of the remaining 18 samples exhibiting Tl isotope compositions significantly heavier than normal mantle. The generally heavy Tl isotope compositions of the lavas are similar to the Tl isotope variation in the sediments outboard of the Aleutian arc (Fig. 2), which clearly implicates sediments as a significant source of Tl in the Aleutians. In detail, however, there are some important systematic along-arc changes in Tl isotopes that provide clues to processes taking place in the sub-arc mantle.

As has been noted previously (Kay and Kay, 1994; Sun, 1980; Yogodzinski et al., 2010), the composition of sediment subducted underneath the Aleutian arc is expected to change from continental detrital in the east as represented by DSDP Site 178 toward compositions with a higher proportion of abyssal clay in the Central Aleutians. Here we have obtained the first data from a drill hole outboard of the Central Aleutians (ODP Hole 886C), which confirms that

584 pelagic clays enriched in trace elements like Nd, Pb and Tl are common at this location.
585 Thallium isotope compositions of sediments in DSDP Sites 178 and 183 and ODP Hole 886C
586 conform to the expected relationship whereby sediments more proximal to the continent display
587 ε^{205}Tl ~ -2, with increasingly heavy Tl isotope compositions as sediment deposition rates decline
588 and therefore contain higher concentrations of authigenic Fe and Mn oxides (Figs. 2 and 6).

589 The clear shift in Tl isotope composition of sediments from ε^{205}Tl ~ -2 outboard of the
590 Eastern Aleutians to ε^{205}Tl > 0 outboard of the Central Aleutians is mirrored by the average Tl
591 isotope compositions of lavas in these locations (Figs. 7 and 8). Although each island appears to
592 preserve some Tl isotope variation outside of analytical uncertainty (Figs. 7 and 8), on average,
593 islands in the Central Aleutians exhibit heavier Tl isotope compositions than do the islands in the
594 Eastern Aleutians. The relationship between Tl isotope compositions in subducted sediments and
595 the extruded lavas indicates that sediment inputs are the main control on Tl isotope compositions
596 of lavas in the Aleutians east of Kanaga Island. This interpretation is corroborated by the inverse
597 correlation observed between Pb and Tl isotopes for the Central and Eastern Aleutian lavas (Fig.
598 7). It is important to note that this inverse correlation does not reflect two-component mixing, but
599 that each point lies on an individual mixing line between the mantle wedge and a unique pelagic-
600 detrital mix.

601 However, the observed trend is generally consistent with the Pb isotopes observed for
602 pelagic clays at ODP 886C that are, on average, less radiogenic than the detrital-dominated
603 sediments at DSDP Sites 178 and 183. Mixing lines between the sub-arc mantle and bulk detrital
604 and pelagic sediments show that the quantity of sediment added from the slab to the sub-arc
605 mantle decreases systematically from the Eastern to the Central Aleutians, which is consistent

606 with the previously inferred subducted sediment flux along the Aleutian arc (Kay and Kay, 1994;
607 Kelemen et al., 2003).

608 This trend is also reproduced in plots of Sr-Tl and Nd-Tl isotopes (Fig. 8), which shows that
609 all four elements are likely dominated by sediment fluxes from the slab. The amount of bulk
610 sediment required to account for the observed Nd, Pb, Sr and Tl isotope variations are
611 consistently ~0.6-1% by weight in the east, while mixing relationships in the Central Aleutians
612 using Nd, $^{206}Pb/^{204}Pb$, Sr and Tl isotopes are consistent with ~0.2-0.6% by weight sediment
613 addition, which is in reasonable agreement with previous work that inferred up to ~2 weight %
614 sediment in the mantle sources of the Aleutian Islands (Kay, 1980; Kay and Kay, 1988; Kay et
615 al., 1978; Kelemen et al., 2003; Yogodzinski et al., 2010). Interestingly, bulk sediment mixing
616 using $^{207}Pb/^{204}Pb$ and $^{208}Pb/^{204}Pb$ (Figs. 7b and 7c) predict significantly smaller (<0.2% by
617 weight) pelagic sediment fractions in the Central Aleutians than do all other isotope ratios.

618 This consistent offset might be explained by addition of a third component with
619 unradiogenic $^{207}Pb/^{204}Pb$ and $^{208}Pb/^{204}Pb$ such as a fluid from AOC (Miller et al., 1994). To
620 maintain the consistent mixing relationships illustrated in Fig. 8, such a fluid would have to be
621 highly enriched in Pb compared with Nd, Sr and Tl. In addition, the $^{206}Pb/^{204}Pb$ of the fluid could
622 not be significantly less radiogenic than 18.6-18.7 in order to preserve the ~0.4% pelagic
623 sediment produced by the mixing relationship in Figure 7a. Alternatively, it is also possible that
624 the average subducted sediment outboard of the Central Aleutians is more affected by the type of
625 highly enriched pelagic sediment represented by 886C-8H-4 58-60cm (Table 4), which is
626 characterized by highly unradiogenic $^{207}Pb/^{204}Pb$ and $^{208}Pb/^{204}Pb$, whereas $^{206}Pb/^{204}Pb$ is only
627 slightly less radiogenic than most of the other pelagic sediment samples from ODP Hole 886C.
628 Hence, if material similar to sample 8H-4 58-60cm represents close to 60% of the subducted

sediment Pb budget the bulk subducted sediment would be characterized by $^{207}Pb/^{204}Pb$ ~ 15.57 and $^{208}Pb/^{204}Pb$ ~ 38.3, which would yield mixing relationships requiring ~0.4% bulk sediment like those observed for Nd, $^{206}Pb/^{204}Pb$, Sr and Tl isotopes. The present fraction of Pb in ODP Hole 886C contributed from the basal pelagic sediment is ~35%, which is based on visual inspection of core barrel photographs (Rea et al., 1993). Although this method of estimating average sediment core compositions is the best available (short of conducting hundreds of individual sediment analyses throughout a core), it carries significant uncertainties for elements such as Pb, Tl, La and Nd that display almost two orders of magnitude concentration variations in individual sediment horizons. Hence, if the sediment thickness and/or average concentration of certain sediment horizons have been under- or overestimated this could lead to large changes in the whole-core average composition.

The similarity in the required sediment component based on Sr, Nd, Pb and Tl isotopes suggests that initial mixing between sediment and mantle does not strongly fractionate these four trace elements. However, it is well documented that Aleutian lavas (and arc lavas in general) display highly fractionated Sr/Nd and Pb/Nd compared with all the bulk input components that enter the subduction zone (Class et al., 2000; Miller et al., 1994). Therefore, there must be one or more processes occurring within the subduction zone that are capable of fractionating trace elements. Combining the evidence from isotope-isotope diagrams and the ubiquitous trace element fractionation in arcs would, therefore, suggest that mixing and trace element fractionation occur in two separate steps. The elemental fractionations of Sr/Nd, Ce/Pb, Th/Nd and others are often inferred to originate from melting or dehydration of slab sediment and/or altered oceanic crust with phases such as allanite, monazite, apatite, phengite, biotite, lawsonite or sulfide in the residue (Hermann and Rubatto, 2009; Johnson and Plank, 1999; Prytulak et al.,

2013). These accessory phases could produce large variations in the transport efficiency of Sr, Nd, Pb and Tl, because of the strong compatibility of Nd in allanite and monazite, Pb in sulfide and apatite, and Tl in sulfide, biotite and phengite. Thus, sediment melts released from the slab into the mantle wedge are likely characterized by fractionated Sr/Nd, Pb/Tl, Sr/Tl and Nd/Tl ratios that would cause strong curvature in the isotope mixing diagrams (Figs. 7 and 8) that is not compatible with the consistent bulk mixing relationships observed.

Of the four isotope systems considered here, reliable experimental data for element partitioning during sediment melting only exists for Sr and Nd (Hermann and Rubatto, 2009; Johnson and Plank, 1999; Skora and Blundy, 2010). These data show that over a range of temperatures (600-1050°C) and sediment compositions, Nd is preferentially retained in the sediment residue (notably by monazite), while Sr is uniformly released into the melt phase. On average, experiments in the temperature range from 700-900°C show that Sr is about 20 times less compatible than Nd during sediment melting, which results in high Sr/Nd ratios in the sediment melts. A potential problem with these experiments is that they were all doped with relatively large amounts of Nd and other REE, which may have stabilized excess abundances of monazite because REE are a main constituent of the mineral. The Nd partition coefficients presented in these studies may, therefore, be higher than for undoped compositions. Irrespective of the absolute partition coefficients, sediment melts are expected to be characterized by higher Sr/Nd ratios than the bulk sediment, which generates significantly different mixing relationships between mantle and sediment melts compared to bulk sediment. Figure 9 shows the effect of the different Nd/Sr ratios in bulk sediment and sediment melts generated by 20% melting of the subducted sediment components in the Eastern and Central Aleutians when using the experimental data currently available in the literature. It is evident that none of the lavas studied

here nor those of other published lavas from the Central and Eastern Aleutians fall within the sediment melt field. Larger degrees of sediment melting (Skora and Blundy, 2010) will move the sediment melt field closer to the bulk sediment field, but even 40% sediment melting will only move a few of the samples into the sediment melt field and then only close to the mixing line with ODP 886C sediment melts.

On the other hand, if monazite abundances for un-doped sediment compositions are lower than doped experiments suggest, then it is likely that degrees of sediment melting around 20-40% will significantly attenuate the Sr/Nd fractionation of the sediment melt because the accessory phases responsible for the elemental fractionation are almost or entirely melted out (Hermann and Rubatto, 2009). In this case, sediment melts will fail to produce the high Sr/Nd ratios (and likely also other trace element ratios that might be governed by residual accessory phases) observed in Aleutian lavas and therefore processes subsequent to mantle-sediment melt mixing would be needed to fractionate trace element ratios like Sr/Nd, Ce/Pb, Cs/Tl and Th/Nd.

Bulk sediment transfer from slab to mantle wedge could be consistent with recent models of sediment transport from the slab to the mantle wedge whereby either pure sediment (Behn et al., 2011) or mélange diapirs (Marschall and Schumacher, 2012) are the primary mode of adding sediments and/or AOC to the source regions of arc lavas. Mélange formation at the slab-mantle interface, which based on field studies is common in subduction zones (Bebout, 1991; King et al., 2003), represents a mixture between slab material (both sediments and AOC) and the mantle wedge. Therefore, average mélange material is expected to plot along bulk mixing lines between mantle and sediment/AOC slab components, similar to what we observe in Figures 7-9.

It is important to note that the isotope-isotope plots (Figs. 7-9) only provide information about the elemental ratios (e.g. Sr/Nd, Tl/Sr, Tl/Nd, Tl/Pb) at the time when the components

mixed. Subsequent trace element fractionation would not be detected in these plots. In other words, models that invoke bulk mixing between mantle and sediment/AOC require that the strong fractionation of trace elements observed in arc lavas, including Sr/Nd, Ce/Pb and Nd/Th, must then occur upstream of the mixing process rather than prior to. Melting of mélange diapirs in the mantle wedge (Marschall and Schumacher, 2012) is a potential means of fractionating trace elements if melting residuals at high temperatures (likely >1100°C) contains the residual phases that may produce the required trace element fractionations. Future experiments and studies of mélange material at subduction zone conditions will need to investigate the viability of these processes in more detail.

6.3. Thallium isotope signature of slab melts from altered oceanic crust

The Tl isotope ratios determined for samples from the Western Aleutians are systematically different from those observed in the Central and Eastern Aleutian Islands. When the two samples affected by assimilation and degassing (TN182_07_005 and TN182_08_003) are excluded, all samples except two fall within a limited range of $\varepsilon^{205}Tl$ = -1.5 to -3.4 (Table 3). Even though this range only represents about four times our long-term reproducibility there is a suggestion that Tl isotopes correlate with both Sr and Pb isotopes, whereby the least radiogenic Sr and Pb isotope compositions are characterized by $\varepsilon^{205}Tl \sim -3.5$ (Figs. 7 and 8). We also find that the Miocene sample from Adak Island, ADK53, falls close to these trends, suggesting that the Western Aleutian lavas were influenced by the same component as ADK53. There is strong evidence that the Western Aleutian lavas as well as ADK53 sample a distinct component of eclogite slab melt (Kay, 1978; Yogodzinski et al., 2015; Yogodzinski et al., 1995) that is characterized by high Sr/Y and Dy/Yb coupled with unradiogenic Pb and Sr isotope compositions. This eclogite melt

likely originates from subducted basaltic oceanic crust that was transformed at depth to eclogite. Conversely, the lack of heavy Tl isotope compositions in the Western Aleutians indicate that sediments do not play a major role for the Tl mass balance of these lavas. This observation is consistent with the strongly attenuated sediment flux underneath the Western Aleutians (Kelemen et al., 2003; Yogodzinski et al., 1994) as well as radiogenic isotope compositions of Western Aleutian samples, which have among the least radiogenic Pb and most radiogenic Nd in the Aleutians. Nonetheless, plots of Pb-Pb and Nd-Pb isotopes as well as Ce/Pb significantly lower than normal mantle imply that minor sediment or fluid components are present in Western Aleutian samples (Yogodzinski et al., 2015). Therefore, simple mixing of melts from eclogitized oceanic crust and the mantle wedge cannot account for the petrogenesis of most Western Aleutian volcanics.

Thallium concentrations and isotope compositions of oceanic crust display distinct and systematic variations with crustal depth (Nielsen et al., 2006c). In particular, the upper volcanic zone is enriched in Tl with distinct $\varepsilon^{205}Tl < -2$. The sheeted dike complex, lower crustal gabbros and ultramafic cumulates, however, are likely very depleted in Tl and exhibit $\varepsilon^{205}Tl \sim -2$, which is indistinguishable from the MORB mantle (Nielsen et al., 2006c). In the Western Aleutian lavas, the proposed eclogite melt endmember is characterized by the lightest Tl isotope compositions suggesting that at least part of the eclogite source region formed from the volcanic zone of the subducted basaltic crust. This inference is also supported by the relatively high Tl concentrations for the putative eclogite component of up to 150 ng/g (Table 3), which would imply a source region containing Tl concentrations significantly in excess of the ~ 1 ng/g Tl observed for the sheeted dike complex (Nielsen et al., 2006c).

One lava from Kanaga Island (S489) is the only sample from the main Aleutian Islands in this study that exhibits $\varepsilon^{205}Tl < -2$, which could be indicative of influence from low-temperature altered oceanic crust. There is no indication based on Sr/Y, Dy/Yb or radiogenic isotope ratios that a significant component derived from slab melting has influenced this sample. However, given the generally attenuated sediment flux needed to account for radiogenic isotope data from the Central Aleutians compared to the Eastern Aleutians (Figs. 7 and 8), it is possible that some volcanoes in the Central Aleutians become more dominated by inputs from dehydrated altered oceanic crust. Such an interpretation would be consistent with the greater range in Tl isotopes observed for Kanaga Island, which could reflect that the relative contributions of Tl from sediments and altered oceanic crust are highly variable when the subducted sediment flux becomes sufficiently small.

6.4. Possible contributions from oceanic crust dehydration

Sediments have been widely implicated as the primary component that causes radiogenic Pb, Sr and Nd isotope variation in the Eastern and Central Aleutians (Kay and Kay, 1988; Kay et al., 1978; Kelemen et al., 2003), which is clearly supported by our new Tl isotope data (Figs. 7 and 8). However, fluids sourced from dehydrating oceanic crust as well as melts from eclogitized oceanic crust may also contribute to lavas in the Central and Eastern Aleutian Islands (Jicha et al., 2004; Miller et al., 1994; Singer et al., 2007; Yogodzinski et al., 2015; Yogodzinski et al., 1995). For example, several studies have suggested that a fluid extracted from AOC can account for the excess Sr in Aleutian lavas (Class et al., 2000; Jicha et al., 2004; Singer et al., 2007). This process is clearly a reasonable way to explain the trace element fractionation of several key trace elements (notably the high Sr/Nd, Pb/Ce and B/La). However, addition of an AOC component

766 would cause Sr isotopes to become slightly more radiogenic (assuming $^{87}Sr/^{86}Sr \sim 0.704$ in the
767 upper ~600 meters of the oceanic crust (Staudigel et al., 1995; Teagle et al., 2003)) whereas Nd
768 would be largely unaffected due to the low solubility of Nd in the fluid phase (Kessel et al.,
769 2005). Adding this 'fluid AOC' component to the sediment melt would move the sediment melt-
770 mantle mixing lines in Figure 9 upwards and therefore even further away from the sediment melt
771 field. On the other hand, if 'fluid AOC' Sr were derived from throughout the oceanic crust (with
772 MORB $^{87}Sr/^{86}Sr \sim 0.7025$) and this fluid exhibited elevated Sr/Nd similar to low degree (<20%)
773 sediment melts, then a mixing line could be produced that is indistinguishable from mantle-bulk
774 sediment mixing, and would intersect the Aleutian arc data. Hence, low degree (<20%) sediment
775 melts are able to explain the Sr-Nd isotope data from the Aleutian arc if they were mixed with
776 AOC fluids characterized by MORB isotope compositions and Sr/Nd ratios similar to the
777 sediment melt. However, this scenario would require that less than 15% of Sr in the Aleutian
778 lavas are derived from the mantle, as otherwise the mixing lines would become too curved to
779 encompass all the isotopic data.

780 It is currently unknown how mobile Tl is in fluids released from the subducting slab and,
781 therefore, it is difficult to quantify what the effect on Tl isotopes and abundances would be if
782 Aleutian lavas contained a significant fluid component from altered oceanic crust. We can obtain
783 qualitative information by examining the relation between the highly fluid mobile element Cs
784 (Kessel et al., 2005; Melzer and Wunder, 2000) and Tl across the Aleutian arc (Fig. 10). All bulk
785 endmembers in the Aleutian arc (e.g. mantle wedge, detrital and pelagic sediments, altered
786 oceanic crust and slab melts) display $Cs/Tl < 10$, while lavas from the Central and Eastern
787 Aleutian Islands display $Cs/Tl = 8\text{-}35$. Although Cs and Tl do not partition identically during
788 mantle melting (Nielsen et al., 2014), they are both so incompatible that mantle melts

789 representing >5% melting are not significantly fractionated from their mantle source. Thallium
790 concentration data from a range of arcs indicates that Tl is only mildly fluid mobile (Noll et al.,
791 1996) and, therefore, fluid dominated arc lavas should display high Cs/Tl. Thus, the high Cs/Tl
792 in Aleutian lavas are potentially caused by addition of a fluid with high Cs/Tl to the magma
793 source region. Alternatively, the high Cs/Tl could be explained by a residual phase in the mantle
794 wedge or the slab that retains Tl over Cs. This residual phase could for example be sulfide or
795 phengite, both of which are expected to accommodate Tl (Kiseeva and Wood, 2013; Nielsen et
796 al., 2014; Prytulak et al., 2013). Phengite also incorporates Cs, but it has been shown that Cs is
797 the least compatible alkali metal in phengite (Hermann and Rubatto, 2009; Melzer and Wunder,
798 2000) due to its slightly larger ionic radius than the alkali metal cation site in phengite (Busigny
799 et al., 2003). The ionic radius of Tl is very similar to that of Rb (Shannon, 1976), which should
800 render Tl significantly more compatible in phengite than Cs. Thus, high Cs/Tl in arc lavas could
801 be due to phengite retention in the slab as well as residual sulfide in the mantle wedge. However,
802 future experimental work must be conducted in order to verify this inference.
803 Conversely, lavas from the Western Aleutians exhibit Cs/Tl that overlaps with MORB (Fig.
804 10) suggesting that the high Cs/Tl component in the main Aleutian Islands is largely absent in
805 the Western Aleutians. Considering that sediment contributions are likely small in the Western
806 Aleutians (Kelemen et al., 2003; Yogodzinski et al., 2015; Yogodzinski et al., 1994), it follows
807 that the high Cs/Tl ratios in the main Aleutian Islands probably originate from the sediment
808 component rather than fluids released from altered oceanic crust. This conclusion is supported by
809 the weak tendency for Eastern and Central Aleutian lavas with heavy Tl isotope compositions to
810 display the highest Cs/Tl (Fig. 10). It should be noted that the process that generated high Cs/Tl
811 in the Aleutian lavas, be it fluid driven or mineralogical, would still need to occur after bulk

812 mixing between the sediment and mantle components due to the mixing relations observed
813 between Tl-Sr-Nd-Pb isotopes (Figs. 7-9). However, given the lack of Tl partitioning data for
814 phengite and subduction fluids it is presently not possible to conclude if fluids are necessary to
815 account for the Cs/Tl ratios observed in the Aleutian lavas.
816

817 ## 7. Conclusions

818 We have conducted the first Tl isotope study of lavas covering the entire Aleutian arc and
819 subducting sediments located outboard of the main Aleutian Islands. Systematic changes are
820 observed in the average sediment Tl isotope composition from ε^{205}Tl ~ -2, similar to the
821 continental crust and upper mantle, in the Eastern Aleutians to ε^{205}Tl ~ +4 in the Central
822 Aleutians, which reflects a significant component of authigenic Mn oxides in these slowly
823 accumulating sediments. Lavas in the Aleutian Islands east of Kanaga generally mirror the trend
824 from ε^{205}Tl ~ -2 in the Eastern Aleutians to ε^{205}Tl ~ +2 in the Central Aleutians caused by the
825 changing subducted sediment composition across the arc. Simple models of sediment-mantle
826 mixing in Nd, Pb, Sr and Tl isotope space reveal that bulk sediment mixed with a depleted
827 mantle source can account for the isotopic variation observed in the Central and Eastern Aleutian
828 Islands. Our results are, therefore, consistent with recent models of sediment transport from the
829 slab to the mantle wedge whereby either pure sediment (Behn et al., 2011) or mélange diapirs
830 (Marschall and Schumacher, 2012) are the primary mode of adding sediments to the source
831 regions of arc lavas. However, bulk sediment mixing models require that processes occurring
832 after sediment-mantle mixing fractionate trace element ratios such as Ce/Pb, Cs/Tl, Sr/Nd, and
833 Th/Nd. Both the sediment and mélange diapir models have not been explored in terms of the
834 resulting chemical signatures that can be generated in these scenarios. For example, it is not clear

835 if sediment diapirs need to melt first in order to effectively mix with the mantle wedge in which
836 case trace element fractionation would likely occur prior to mixing and, therefore, not adequately
837 explain the isotope-isotope relationships (Fig. 9). The strong heterogeneity of mélange zones
838 sometimes observed in the field (Bebout, 2007) is perhaps not compatible with the relatively
839 homogenous isotopic signatures often observed for individual aleutian volcanoes (Kelemen et
840 al., 2003). Lastly, the high temperatures (>1100°C) potentially experienced by sediment and
841 mélange diapirs in the mantle wedge could prevent significant trace element fractionation as
842 accessory phases might melt out and therefore not generate the required trace element
843 fractionation. Future experiments that reproduce the conditions experienced in sediment and
844 mélange diapirs will need to investigate the viability of these processes in generating the
845 observed major and trace element characteristics of arc lavas.

846 Alternative models that involve sediment melting in excess of 50% may also be compatible
847 with the presented Nd, Pb, Sr and Tl isotopes. Such large degrees of melting could be driven by
848 an influx of AOC fluid with MORB-like isotope compositions (Skora and Blundy, 2010), which
849 may also deliver fractionated trace elements. Provided the sediment melt and AOC fluid had
850 similar trace element ratios, they have the potential to produce arrays that look like bulk mixing
851 but also generate trace element fractionations (e.g., high Sr/Nd, Cs/Tl and Pb/Ce) observed in arc
852 lavas.

853 Thallium isotope systematics in Western Aleutian lavas show compositions slightly lighter
854 than the upper mantle, which implies a negligible sediment flux at this location and probably
855 involvement of low-temperature altered oceanic crust in the generation of these lavas. In general,
856 the lightest Tl isotope compositions are observed for the highest Sr/Y ratios and most

unradiogenic Sr and Pb isotope compositions, which may be consistent with derivation of these lavas via melting of eclogitized altered oceanic crust.

8. Acknowledgements

This study used samples recovered during the Ocean Drilling Program. This study was funded by NSF grants EAR-1119373 and -1427310 to SGN and EAR-1456814 to TP. We thank Daniel Rasmussen and Louise Bolge for their chemistry lab and ICP-MS talents in analyzing elemental concentrations in ODP 886 sediments. We also thank Merry Cai for sharing Aleutian data compilations, Peter Kelemen for discussions and Oliver Nebel and an anonymous reviewer for insightful comments that helped improve this manuscript.

9. References

Abouchami, W., Galer, S.J.G., Koschinsky, A., 1999. Pb and Nd isotopes in NE Atlantic Fe-Mn crusts: Proxies for trace metal paleosources and paleocean circulation. Geochim. Cosmochim. Acta. 63, 1489-1505.

Adam, J., Green, T., 2006. Trace element partitioning between mica- and amphibole-bearing garnet lherzolite and hydrous basanitic melt: 1. Experimental results and the investigation of controls on partitioning behaviour. Contrib. Mineral. Petrol. 152, 1-17.

Baker, R.G.A., Rehkämper, M., Hinkley, T.K., Nielsen, S.G., Toutain, J.P., 2009. Investigation of thallium fluxes from subaerial volcanism-Implications for the present and past mass balance of thallium in the oceans. Geochim. Cosmochim. Acta. 73, 6340-6359.

Bebout, G.E., 1991. Field-Based Evidence for Devolatilization in Subduction Zones - Implications for Arc Magmatism. Science 251, 413-416.

Bebout, G.E., 2007. Metamorphic chemical geodynamics of subduction zones. Earth Planet. Sci. Lett. 260, 373-393.

Behn, M.D., Kelemen, P.B., Hirth, G., Hacker, B.R., Massonne, H.J., 2011. Diapirs as the source of the sediment signature in arc lavas. Nature Geoscience 4, 641-646.

Ben Othmann, D., White, W.M., Patchett, J., 1989. The geochemistry of marine sediments, island arc magma genesis, and crust-mantle recycling. Earth Planet. Sci. Lett. 94, 1-21.

Busigny, V., Cartigny, P., Philippot, P., Ader, M., Javoy, M., 2003. Massive recycling of nitrogen and other fluid-mobile elements (K, Rb, Cs, H) in a cold slab environment: evidence from HP to UHP oceanic metasediments of the Schistes Lustres nappe (western Alps, Europe). Earth Planet. Sci. Lett. 215, 27-42.

890 Byrne, R.H., 2002. Inorganic speciation of dissolved elements in seawater: the influence of pH
891 on concentration ratios. Geochemical Transactions 3, 11-16.
892 Carpentier, M., Chauvel, C., Mattielli, N., 2008. Pb–Nd isotopic constraints on sedimentary input
893 into the Lesser Antilles arc system. Earth Planet. Sci. Lett. 272, 199-211.
894 Carter, L.B., Skora, S., Blundy, J.D., De Hoog, J.C.M., Elliott, T., 2015. An Experimental Study
895 of Trace Element Fluxes from Subducted Oceanic Crust. J. Petrol. 56, 1585-1605.
896 Class, C., Miller, D.M., Goldstein, S.L., Langmuir, C.H., 2000. Distinguishing melt and fluid
897 subduction components in Umnak Volcanics, Aleutian Arc. Geochem. Geophys. Geosyst.
898 1, doi:10.1029/1999GC000010.
899 Coggon, R.M., Rehkämper, M., Atteck, C., Teagle, D.A.H., Alt, J.C., Cooper, M.J., 2014.
900 Mineralogical and Microbial Controls on Thallium Uptake During Hydrothermal
901 Alteration of the Upper Ocean Crust. Geochim. Cosmochim. Acta. 144, 25-42.
902 Defant, M.J., Drummond, M.S., 1990. Derivation of Some Modern Arc Magmas by Melting of
903 Young Subducted Lithosphere. Nature 347, 662-665.
904 George, R., Turner, S., Hawkesworth, C., Morris, J., Nye, C., Ryan, J., Zheng, S.H., 2003.
905 Melting processes and fluid and sediment transport rates along the Alaska-Aleutian arc
906 from an integrated U-Th-Ra-Be isotope study. J. Geophys. Res.-Solid Earth 108.
907 Hegner, E., Tatsumoto, M., 1987. Pb, Sr, and Nd Isotopes in Basalts and Sulfides from the Juan-
908 De-Fuca Ridge. J. Geophys. Res.-Solid Earth and Planets 92, 11380-11386.
909 Hein, J.R., Koschinsky, A., Bau, M., Manheim, F.T., Kang, J.-K., Roberts, L., 2000. Cobalt-rich
910 ferromanganese crusts in the Pacific, in: Cronan, D.S. (Ed.), Handbook of Marine
911 Mineral Deposits. CRC Press, Boca Raton, pp. 239-280.
912 Heinrichs, H., Schulz-Dobrick, B., Wedepohl, K.H., 1980. Terrestrial Geochemistry of Cd, Bi,
913 Tl, Pb, Zn and Rb. Geochim. Cosmochim. Acta. 44, 1519-1533.
914 Hermann, J., 2002. Allanite: thorium and light rare earth element carrier in subducted crust.
915 Chem. Geol. 192, 289-306.
916 Hermann, J., Rubatto, D., 2009. Accessory phase control on the trace element signature of
917 sediment melts in subduction zones. Chem. Geol. 265, 512-526.
918 Jackson, M.G., Hart, S.R., 2006. Strontium isotopes in melt inclusions from Samoan basalts:
919 Implications for heterogeneity in the Samoan plume. Earth Planet. Sci. Lett. 245, 260-
920 277.
921 Jenner, F.E., O'Neill, H.S.C., 2012. Analysis of 60 elements in 616 ocean floor basaltic glasses.
922 Geochem. Geophys. Geosyst. 13.
923 Jicha, B.R., Singer, B.S., Brophy, J.G., Fournelle, J.H., Johnson, C.M., Beard, B.L., Lapen, T.J.,
924 Mahlen, N.J., 2004. Variable impact of the subducted slab on Aleutian island arc magma
925 sources: Evidence from Sr, Nd, Pb, and Hf isotopes and trace element abundances. J.
926 Petrol. 45, 1845-1875.
927 Jochum, K.P., Verma, S.P., 1996. Extreme enrichment of Sb, Tl and other trace elements in
928 altered MORB. Chem. Geol. 130, 289-299.
929 Johnson, M.C., Plank, T., 1999. Dehydration and melting experiments constrain the fate of
930 subducted sediments. Geochem. Geophys. Geosyst. 1.
931 Kay, R.W., 1978. Aleutian magnesian andesites - melts from subducted Pacific ocean crust. J.
932 Volcanol. Geotherm. Res. 4, 117-132.
933 Kay, R.W., 1980. Volcanic Arc Magmas - Implications of a Melting-Mixing Model for Element
934 Recycling in the Crust-Upper Mantle System. J Geol 88, 497-522.

Kay, R.W., Kay, S.M., 1988. Crustal Recycling and the Aleutian Arc. Geochim. Cosmochim. Acta. 52, 1351-1359.
Kay, R.W., Sun, S.S., Lee-Hu, C.N., 1978. Pb and Sr isotopes in volcanic rocks from the Aleutian Islands and Pribilof Islands, Alaska. Geochim. Cosmochim. Acta. 42, 263-273.
Kay, S.M., Kay, R.W., 1994. Aleutian magmas in space and time, in: Plafker, G., Berg, H.C. (Eds.), The geology of Alaska. Geological Society of America, pp. 687-722.
Kelemen, P.B., Yogodzinski, G.M., Scholl, D.W., 2003. Along-strike Variation in Lavas of the Aleutian Island Arc: Implications for the Genesis of High Mg# Andesite and the Continental Crust. Geophysical Monograph 138, 223-276.
Kessel, R., Schmidt, M.W., Ulmer, P., Pettke, T., 2005. Trace element signature of subduction-zone fluids, melts and supercritical liquids at 120-180 km depth. Nature 437, 724-727.
King, R.L., Kohn, M.J., Eiler, J.M., 2003. Constraints on the petrologic structure of the subduction zone slab-mantle interface from Franciscan Complex exotic ultramafic blocks. Geological Society of America Bulletin 115, 1097-1109.
Kiseeva, E.S., Wood, B.J., 2013. A simple model for chalcophile element partitioning between sulphide and silicate liquids with geochemical applications. Earth Planet. Sci. Lett. 383, 68-81.
Ling, H.F., Burton, K.W., Onions, R.K., Kamber, B.S., vonBlanckenburg, F., Gibb, A.J., Hein, J.R., 1997. Evolution of Nd and Pb isotopes in Central Pacific seawater from ferromanganese crusts. Earth Planet. Sci. Lett. 146, 1-12.
Ling, H.F., Jiang, S.Y., Frank, M., Zhou, H.Y., Zhou, F., Lu, Z.L., Chen, X.M., Jiang, Y.H., Ge, C.D., 2005. Differing controls over the Cenozoic Pb and Nd isotope evolution of deepwater in the central North Pacific Ocean. Earth Planet. Sci. Lett. 232, 345-361.
Lugmair, G.W., Galer, S.J.G., 1992. Age and Isotopic Relationships among the Angrites Lewis Cliff-86010 and Angra-Dos-Reis. Geochim. Cosmochim. Acta. 56, 1673-1694.
Marschall, H.R., Schumacher, J.C., 2012. Arc magmas sourced from melange diapirs in subduction zones. Nature Geoscience 5, 862-867.
Melzer, S., Wunder, B., 2000. Island-arc basalt alkali ratios: Constraints from phengite-fluid partitioning experiments. Geology 28, 583-586.
Miller, D.M., Goldstein, S.L., Langmuir, C.H., 1994. CERIUM LEAD AND LEAD-ISOTOPE RATIOS IN ARC MAGMAS AND THE ENRICHMENT OF LEAD IN THE CONTINENTS. Nature 368, 514-520.
Morris, J.D., Leeman, W.P., Tera, F., 1990. The subducted component in island-arc lavas - constraints from Be isotopes and B-Be systematics. Nature 344, 31-36.
Nielsen, S.G., Gannoun, A., Marnham, C., Burton, K.W., Halliday, A.N., Hein, J.R., 2011. New age for ferromanganese crust 109D-C and implications for isotopic records of lead, neodymium, hafnium, and thallium in the Pliocene Indian Ocean. Paleoceanography 26, PA2213, doi:2210.1029/2010PA002003.
Nielsen, S.G., Klein, F., Kading, T., Blusztajn, J., Wickham, K., 2015. Thallium as a Tracer of Fluid-Rock Interaction in the Shallow Mariana Forearc. Earth Planet. Sci. Lett. 430, 416-426.
Nielsen, S.G., Mar-Gerrison, S., Gannoun, A., LaRowe, D., Klemm, V., Halliday, A.N., Burton, K.W., Hein, J.R., 2009. Thallium isotope evidence for a permanent increase in marine organic carbon export in the early Eocene. Earth Planet. Sci. Lett. 278, 297-307.

Nielsen, S.G., Rehkämper, M., 2011. Thallium isotopes and their application to problems in earth and environmental science, in: Baskaran, M. (Ed.), Handbook of Environmental Isotope Geochemistry. Springer, pp. 247-270.

Nielsen, S.G., Rehkämper, M., Baker, J., Halliday, A.N., 2004. The precise and accurate determination of thallium isotope compositions and concentrations for water samples by MC-ICPMS. Chem. Geol. 204, 109-124.

Nielsen, S.G., Rehkämper, M., Brandon, A.D., Norman, M.D., Turner, S., O'Reilly, S.Y., 2007. Thallium isotopes in Iceland and Azores lavas - Implications for the role of altered crust and mantle geochemistry. Earth Planet. Sci. Lett. 264, 332-345.

Nielsen, S.G., Rehkämper, M., Halliday, A.N., 2006a. Large thallium isotopic variations in iron meteorites and evidence for lead-205 in the early solar system. Geochim. Cosmochim. Acta. 70, 2643-2657.

Nielsen, S.G., Rehkämper, M., Norman, M.D., Halliday, A.N., Harrison, D., 2006b. Thallium isotopic evidence for ferromanganese sediments in the mantle source of Hawaiian basalts. Nature 439, 314-317.

Nielsen, S.G., Rehkämper, M., Porcelli, D., Andersson, P., Halliday, A.N., Swarzenski, P.W., Latkoczy, C., Gunther, D., 2005. Thallium isotope composition of the upper continental crust and rivers - An investigation of the continental sources of dissolved marine thallium. Geochim. Cosmochim. Acta. 69, 2007-2019.

Nielsen, S.G., Rehkämper, M., Teagle, D.A.H., Alt, J.C., Butterfield, D., Halliday, A.N., 2006c. Hydrothermal fluid fluxes calculated from the isotopic mass balance of thallium in the ocean crust. Earth Planet. Sci. Lett. 251, 120-133.

Nielsen, S.G., Shimizu, N., Lee, C.T.A., Behn, M., 2014. Chalcophile behavior of thallium during MORB melting and implications for the sulfur content of the mantle. Geochem. Geophys. Geosyst. 15, 4905-4919.

Nielsen, S.G., Wasylenki, L.E., Rehkämper, M., Peacock, C.L., Xue, Z., Moon, E.M., 2013. Towards an understanding of thallium isotope fractionation during adsorption to manganese oxides. Geochim. Cosmochim. Acta. 117, 252-265.

Noll, P.D., Newsom, H.E., Leeman, W.P., Ryan, J.G., 1996. The role of hydrothermal fluids in the production of subduction zone magmas: Evidence from siderophile and chalcophile trace elements and boron. Geochim. Cosmochim. Acta. 60, 587-611.

Peacock, C.L., Moon, E.M., 2012. Oxidative scavenging of thallium by birnessite: Controls on thallium sorption and stable isotope fractionation in marine ferromanganese precipitates. Geochim. Cosmochim. Acta. 84, 297-313.

Plank, T., 2005. Constraints from thorium/lanthanum on sediment recycling at subduction zones and the evolution of the continents. J. Petrol. 46, 921-944.

Plank, T., Langmuir, C.H., 1998. The chemical composition of subducting sediment and its consequences for the crust and mantle. Chem. Geol. 145, 325-394.

Prytulak, J., Nielsen, S.G., Plank, T., Barker, M., Elliott, T., 2013. Assessing the utility of thallium and thallium isotopes for tracing subduction zone inputs to the Mariana arc. Chem. Geol. 345, 139-149.

Rabinowitz, H.S., Savage, H.M., Plank, T., Polissar, P.J., Kirkpatrick, J.D., Rowe, C.D., 2015. Multiple major faults at the Japan Trench: Chemostratigraphy of the plate boundary at IODP Exp. 343: JFAST. Earth Planet. Sci. Lett. 423, 57-66.

Rea, D.K., Basov, I.A., Janecek, T.R., Palmer-Julson, A., 1993. Sites 885/886. Proceedings of the Ocean Drilling Program, Initial Reports 145, 303-334.

1025 Rehkämper, M., Frank, M., Hein, J.R., Halliday, A., 2004. Cenozoic marine geochemistry of
1026 thallium deduced from isotopic studies of ferromanganese crusts and pelagic sediments.
1027 Earth Planet. Sci. Lett. 219, 77-91.
1028 Rehkämper, M., Frank, M., Hein, J.R., Porcelli, D., Halliday, A., Ingri, J., Liebetrau, V., 2002.
1029 Thallium isotope variations in seawater and hydrogenetic, diagenetic, and hydrothermal
1030 ferromanganese deposits. Earth Planet. Sci. Lett. 197, 65-81.
1031 Rehkämper, M., Halliday, A.N., 1999. The precise measurement of Tl isotopic compositions by
1032 MC- ICPMS: Application to the analysis of geological materials and meteorites.
1033 Geochim. Cosmochim. Acta. 63, 935-944.
1034 Ryan, J.G., Chauvel, C., 2014. 3.13 - The Subduction-Zone Filter and the Impact of Recycled
1035 Materials on the Evolution of the Mantle, in: Turekian, H.D.H.K. (Ed.), Treatise on
1036 Geochemistry (Second Edition). Elsevier, Oxford, pp. 479-508.
1037 Schauble, E.A., 2007. Role of nuclear volume in driving equilibrium stable isotope fractionation
1038 of mercury, thallium, and other very heavy elements. Geochim. Cosmochim. Acta. 71,
1039 2170-2189.
1040 Scher, H.D., Delaney, M.L., 2010. Breaking the glass ceiling for high resolution Nd isotope
1041 records in early Cenozoic paleoceanography. Chem. Geol. 269, 329-338.
1042 Schiano, P., Dupré, B., Lewin, E., 1993. Application of element concentration variability to the
1043 study of basalt alteration (Fangataufa atoll, French Polynesia). Chem. Geol. 104, 99-124.
1044 Shannon, R.D., 1976. Revised effective ionic radii and systematic studies of interatomic
1045 distances in halides and chalcogenides. Acta Crystallographica A32, 751-767.
1046 Shaw, D.M., 1952. The geochemistry of thallium. Geochim. Cosmochim. Acta. 2, 118-154.
1047 Singer, B.S., Jicha, B.R., Leeman, W.P., Rogers, N.W., Thirlwall, M.F., Ryan, J., Nicolaysen,
1048 K.E., 2007. Along-strike trace element and isotopic variation in Aleutian Island arc
1049 basalt: Subduction melts sediments and dehydrates serpentine. J. Geophys. Res.-Solid
1050 Earth 112.
1051 Skora, S., Blundy, J., 2010. High-pressure Hydrous Phase Relations of Radiolarian Clay and
1052 Implications for the Involvement of Subducted Sediment in Arc Magmatism. J. Petrol.
1053 51, 2211-2243.
1054 Snoeckx, H., Rea, D.K., Jones, C.E., Lynn Ingram, B., 1995. EOLIAN AND SILICA
1055 DEPOSITION IN THE CENTRAL NORTH PACIFIC: RESULTS FROM SITES
1056 885/886. Proceedings Of the Ocean Drilling Program, Scientific Results 145, 219-230.
1057 Staudigel, H., Davies, G.R., Hart, S.R., Marchant, K.M., Smith, B.M., 1995. Large scale isotopic
1058 Sr, Nd and O isotopic anatomy of altered oceanic crust: DSDP/ODP sites 417/418. Earth
1059 Planet. Sci. Lett. 130, 169-185.
1060 Sun, S.S., 1980. Lead Isotopic Study of Young Volcanic-Rocks from Mid-Ocean Ridges, Ocean
1061 Islands and Island Arcs. Philosophical Transactions of the Royal Society a-Mathematical
1062 Physical and Engineering Sciences 297, 409-445.
1063 Tanaka, T., Togashi, S., Kamioka, H., Amakawa, H., Kagami, H., Hamamoto, T., Yuhara, M.,
1064 Orihashi, Y., Yoneda, S., Shimizu, H., Kunimaru, T., Takahashi, K., Yanagi, T., Nakano,
1065 T., Fujimaki, H., Shinjo, R., Asahara, Y., Tanimizu, M., Dragusanu, C., 2000. JNdi-1: a
1066 neodymium isotopic reference in consistency with LaJolla neodymium. Chem. Geol. 168,
1067 279-281.
1068 Teagle, D.A.H., Bickle, M.J., Alt, J.C., 2003. Recharge flux to ocean-ridge black smoker
1069 systems: a geochemical estimate from ODP Hole 504B. Earth Planet. Sci. Lett. 210, 81-
1070 89.

Tera, F., Brown, L., Morris, J., Sacks, I.S., Klein, J., Middleton, R., 1986. SEDIMENT INCORPORATION IN ISLAND-ARC MAGMAS - INFERENCES FROM BE-10. Geochim. Cosmochim. Acta. 50, 535-550.

Thirlwall, M.F., Graham, A.M., Arculus, R.J., Harmon, R.S., Macpherson, C.G., 1996. Resolution of the effects of crustal assimilation, sediment subduction, and fluid transport in island arc magmas: Pb-Sr-Nd- O isotope geochemistry of Grenada, Lesser Antilles. Geochim. Cosmochim. Acta. 60, 4785-4810.

Todt, W., Cliff, R.A., Hanser, A., Hofmann, A.W., 1996. Evaluation of a 202Pb–205Pb double spike for high-precision lead isotope analysis. American Geophysical Union Monograph 95, 429-437.

Vervoort, J.D., Plank, T., Prytulak, J., 2011. The Hf-Nd isotopic composition of marine sediments. Geochim. Cosmochim. Acta. 75, 5903-5926.

Von Drach, V., Marsh, B.D., Wasserburg, G.J., 1986. Nd and Sr Isotopes in the Aleutians - Multicomponent Parenthood of Island-Arc Magmas. Contrib. Mineral. Petrol. 92, 13-34.

Von Huene, R., Scholl, D.W., 1991. Observations at Convergent Margins Concerning Sediment Subduction, Subduction Erosion, and the Growth of Continental-Crust. Rev. Geophys. 29, 279-316.

Wedepohl, K.H., 1995. The composition of the continental crust. Geochim. Cosmochim. Acta. 59, 1217-1232.

Weis, D., Kieffer, B., Maerschalk, C., Barling, J., de Jong, J., Williams, G.A., Hanano, D., Pretorius, W., Mattielli, N., Scoates, J.S., Goolaerts, A., Friedman, R.M., Mahoney, J.B., 2006. High-precision isotopic characterization of USGS reference materials by TIMS and MC-ICP-MS. Geochem. Geophys. Geosyst. 7.

Weis, D., Kieffer, B., Maerschalk, C., Pretorius, W., Barling, J., 2005. High-precision Pb-Sr-Nd-Hf isotopic characterization of USGS BHVO-1 and BHVO-2 reference materials. Geochem. Geophys. Geosyst. 6.

White, W.M., Dupré, B., 1986. Sediment subduction and magma genesis in the Lesser Antilles: Isotopic and trace element constraints. Journal of Geophysical Research 91, 5927-5941.

Workman, R.K., Hart, S.R., 2005. Major and trace element composition of the depleted MORB mantle (DMM). Earth Planet. Sci. Lett. 231, 53-72.

Yogodzinski, G.M., Brown, S.T., Kelemen, P.B., Vervoort, J.D., Portnyagin, M., Sims, K.W.W., Hoernle, K., Jicha, B.R., Werner, R., 2015. The Role of Subducted Basalt in the Source of Island Arc Magmas: Evidence from Seafloor Lavas of the Western Aleutians. J. Petrol. 56, 441-492.

Yogodzinski, G.M., Kay, R.W., Volynets, O.N., Koloskov, A.V., Kay, S.M., 1995. Magnesian Andesite in the Western Aleutian Komandorsky Region - Implications for Slab Melting and Processes in the Mantle Wedge. Geological Society of America Bulletin 107, 505-519.

Yogodzinski, G.M., Lees, J.M., Churikova, T.G., Dorendorf, F., Woerner, G., Volynets, O.N., 2001. Geochemical evidence for the melting of subducting oceanic lithosphere at plate edges. Nature 409, 500-504.

Yogodzinski, G.M., Vervoort, J.D., Brown, S.T., Gerseny, M., 2010. Subduction controls of Hf and Nd isotopes in lavas of the Aleutian island arc. Earth Planet. Sci. Lett. in press.

Yogodzinski, G.M., Volynets, O.N., Koloskov, A.V., Seliverstov, N.I., Matvenkov, V.V., 1994. Magnesian Andesites and the Subduction Component in a Strongly Calc-Alkaline Series at Piip Volcano, Far Western Aleutians. J. Petrol. 35, 163-204.

Figure captions

Figure 1: Map of the Aleutian arc. Arrows indicate the locations of the lavas analyzed in this study. The colors used for the different lava locations are repeated throughout all the subsequent figures in this paper where lavas from multiple locations are plotted. Also shown are the three sediment drill cores investigated in order to characterize the sediment input flux to the arc.

Figure 2: Thallium isotope composition and concentration for individual sediment samples from DSDP 178 (dark green), DSDP 183 (light green) and ODP 886C (blue). These colors mimic those used for the lavas whereby the eastern-most sediment core is dark green followed by light green and blue. The large symbols indicate the concentration weighted average Tl isotope compositions and concentrations for each of the three sediment cores. Although DSDP 183 and ODP 886C both contain pelagic components with heavy Tl isotopes and detrital components with ε^{205}Tl ~ -2, ODP 886C clearly is much more dominated by the pelagic components than DSDP 183.

Figure 3: Ce/Tl ratios plotted against Tl isotope composition for all Aleutian lavas investigated in this study. Also shown is the depleted mid ocean ridge basalt mantle (DMM) as well as the average compositions for detrital (DSDP 178 and 183) and pelagic (ODP 886C) sediments. Note that the legend colors follow that of the map in figure 1 and is the same for all subsequent figures with lavas from multiple locations.

Figure 4: Ce/Tl plotted against Th/Rb for all subaerial lavas analyzed in this study. Subaerial aqueous alteration of basaltic lavas preferentially removes alkali metals and given the similarity of the ionic charge and radius between Tl and the alkali metals similar loss of Tl is likely during subaerial alteration. Hence, samples with high Ce/Tl and Th/Rb are probably affected by post eruption alteration (see text for further details).

Figure 5: Potassium plotted against Tl concentrations in lavas from Korovin volcano. Samples broadly follow a fractional crystallization trend. The two arrows indicate the evolution of primitive magmas from fractional crystallization assuming partition coefficients for K and Tl of 0.

Figure 6: Charts showing the Tl isotopic composition of sediments from the three drill holes investigated as a function of depth. It is evident that sediment cores located further west, and thereby more distally to the continent, contain more sections with Tl isotope compositions that are heavier than the continental crust. Grey bars denote the Tl isotope composition of the continental crust and upper mantle (Nielsen et al., 2006b; Nielsen et al., 2005).

Figure 7: Thallium isotopes plotted against Pb isotope ratios. Only samples that are not affected by subaerial weathering, assimilation, contamination or degassing are shown (see text for details). Symbol colors as in figure 3. Also shown are mixing lines between depleted mantle and bulk detrital (DSDP 178 and 183) and pelagic (ODP 886C) sediments. Dashed lines of constant sediment addition are indicated at 0.2% by weight intervals. The Pb isotope composition of the depleted mantle was taken from the most proximal MORB sample, which is

from the northern Juan de Fuca ridge (Hegner and Tatsumoto, 1987). A Pb concentration of 28 ng/g for the DMM is used, which is based on Ce/Tl_{DMM} = 1110 and Pb/Tl_{DMM} = 56 (Nielsen et al., 2014) and a Ce concentration of 0.55 μg/g (Workman and Hart, 2005). The Tl isotope composition of the upper mantle is $\varepsilon^{205}Tl$ = -2 (Nielsen et al., 2006b). The Pb isotope compositions and concentrations for detrital (DSDP 178 and 183) sediments were taken from (Plank and Langmuir, 1998), whereas Pb data for pelagic (ODP 886C) sediment as well as all sedimentary Tl data was taken from Table 5 in this study.

Figure 8: Thallium isotopes plotted against (a) Sr and (b) Nd isotope ratios. Only samples that are not affected by subaerial weathering, assimilation, contamination or degassing are shown (see text for details). Symbol colors as in figure 3. Grey areas denote the Western Aleutian samples except one (for Sr isotopes) or three (for Nd isotopes) outliers. Also shown are mixing lines between depleted mantle and bulk detrital (DSDP 178 and 183) and pelagic (ODP 886C) sediments. Dashed lines of constant sediment addition are indicated at 0.2% by weight intervals. The Nd and Sr isotope composition of the depleted mantle was taken from the most proximal MORB sample, which is from the northern Juan de Fuca ridge (Hegner and Tatsumoto, 1987). Concentrations in the DMM of Sr = 7.66 μg/g and Nd = 0.58 μg/g were used, which were taken from Workman and Hart (2005). The Tl isotope composition of the upper mantle is $\varepsilon^{205}Tl$ = -2 and the Tl content of the DMM was inferred from Pb/Tl ~ 56 (Nielsen et al., 2014). The Nd and Sr isotope compositions and concentrations for detrital (DSDP 178 and 183) sediments were taken from (Plank and Langmuir, 1998; Vervoort et al., 2011), whereas Nd and Sr data for pelagic (ODP 886C) sediment as well as all sedimentary Tl data was taken from Table 5 in this study.

Figure 9: Nd and Sr isotope compositions plotted against each other. Symbol colors as in figure 3, except the Western Aleutian samples that are denoted by grey area. Additional data from previous studies of the Aleutian Islands east of Kanaga are plotted for comparison (Class et al., 2000; George et al., 2003; Jicha et al., 2004; Singer et al., 2007; Yogodzinski et al., 2010). Also shown are mixing lines (bold lines) between depleted mantle and bulk detrital (DSDP 178 and 183) and pelagic (ODP 886C) sediments. Thin dashed lines of constant sediment addition are indicated at 0.2% by weight intervals. The Nd and Sr isotope composition of the depleted mantle was taken from the most proximal MORB sample, which is from the northern Juan de Fuca ridge (Hegner and Tatsumoto, 1987). Concentrations in the DMM of Sr = 7.66μg/g and Nd = 0.58 μg/g were used, which were taken from Workman and Hart (2005).

A second set of bold dashed mixing lines between DMM and sediment melts are also shown. These mixing lines were constructed by generating 20% melts from the detrital and pelagic sediment endmembers and using melt-residue partition coefficients of D_{Sr} = 7.3 and D_{Nd} = 0.35, which represents the average values recorded in sediment melting experiments by Hermann and Rubatto (2009) with temperatures from 750-900°C.

Figure 10: Thallium isotope compositions plotted against Cs/Tl ratio for Aleutian lavas from this study. Only samples that are not affected by subaerial weathering, assimilation, contamination or degassing are shown (see text for details). Symbol colors as in figure 3. Also shown are the values for detrital (DSDP 178 and 183) and pelagic (ODP 886C) sediments as well as an estimated value for altered oceanic crust (AOC) (Nielsen et al., 2006c) and the DMM (Nielsen et al., 2006b; Nielsen et al., 2014). It is notable that many of the Central and Eastern

1211 Aleutian lavas display Cs/Tl higher than any of the bulk components contributing to the lavas.
1212 This effect could either be explained by the involvement of Cs-rich fluids or preferential
1213 retention of Tl in phengite (see text for details).
1214

Table 1: Samples selected from ODP 886C

ODP sample ID	Depth (mbsf)	Lithology	Unit	Unit density (g/cm^3)	Unit thickness (m)
1H 3 60-62cm	3.61	Reddish brown clay	1		
1H 4 70-72cm	5.21	Reddish brown clay	1	1.5	6.8
2H 1 55-57cm	7.36	Dark brown spicule clay	2		
2H 4 65-67cm	11.96	Light brown spicule clay	2		
3H 1 90-92cm	17.21	Brown diatom clay	2	1.45	15.4
3H 5 60-62cm	22.91	Light brown diatom ooze	3		
4H 1 80-82cm	26.61	Light brown diatom ooze	3		
4H 5 30-32cm	30.61	Light brown diatom ooze	3		
5H 1 50-52cm	35.81	Light brown diatom ooze	3		
5H 3 45-47cm	38.76	Light brown diatom ooze	3		
6H 2 70-72cm	47.01	Light brown diatom ooze	3	1.4	26.5
6H 3 120-122cm	49.01	Mn nodule	4	4	0.2
7H 3 58-60cm	57.89	Dark brown clay	5		
7H 5 73-75cm	61.04	Dark brown clay	5	1.5	15
8H 1 48-50cm	64.29	Dark brown clay	6		
8H 4 58-60cm	68.89	Dark brown clay	6	1.55	8.5

1218 Table 5: Weighted average subducted sediment components

Parameter*	East Aleutian Sediment#	Cent. Aleutian Sediment
Rb	57	77.1
Cs	3.4	7.1
Sr	245	203
Ba	2074	3910
La	18.0	58.8
Ce	39.0	103
Nd	19.1	75.7
Tl	0.31	2.25
Pb	12.9	39.6
Th	5.5	11.4
U	2.4	2.23
$^{87}Sr/^{88}Sr$	0.7064	0.711
$^{143}Nd/^{144}Nd$	0.51261	0.5124
$^{206}Pb/^{204}Pb$	19.04	18.61
$^{207}Pb/^{204}Pb$	15.63	15.61
$^{208}Pb/^{204}Pb$	38.69	38.60
$\varepsilon^{205}Tl$	-2.0	3.9

1219 * - concentrations in μg/g

1220 # - Eastern Aleutian sediment composition from Plank & Langmuir, 1998 except Nd isotope

1221 composition from Vervoort et al. (2011) and Tl concentrations and isotopes (this study).

Table 2

Table 2: Tl, Sr, Nd and Pb isotopes for Main Arc lavas

Sample	Eps 205 Tl	Tl [ng/g]	n	87Sr/86Sr	143Nd/144Nd	206Pb/204Pb	207Pb/204Pb	208Pb/204Pb
Kanaga 514	0.2	20	1	0.70307	0.51303	18.731	15.545	38.259
repeat	0.5	31	2					
Kanaga 58	-1.6	199	1	0.70330	0.51304	18.802	15.558	38.347
Kanaga S489	-3.4	24	1	0.70307	0.51301	18.734	15.548	38.267
repeat	-4.1	25	2					
Kanaga S508	0.8	40	1	0.70308	0.51302	18.731	15.548	38.268
Moffett 18 - 15A	1.2	26	1	0.70312	0.51300	18.710	15.538	38.220
Moffett 18-15B	1.3	32	1	0.70312	0.51301	18.709	15.539	38.222
Moffett 2A	2.6	43	1	0.70314	0.51299	18.705	15.540	38.220
Moffett 81 19A	1.8	37	1	0.70315	0.51302	18.731	15.545	38.260
Moffett ADK53*	-3.3	34	1	*0.70285*	*0.51309*	*18.462*	*15.499*	*37.964*
Okmok UM-10	0.7	36	1	0.70303	0.51304	18.726	15.545	38.245
Okmok UM-21	-1.7	91	1	0.70325	0.51304	18.877	15.569	38.415
Okmok UM-23	-0.5	97	1	0.70326	0.51303	18.865	15.566	38.404
Okmok UM-5	-0.2	59	1	0.70329	0.51302	18.887	15.570	38.430
repeat	-0.2	60	2					
Westdahl SAR -4	-2.1	170	1	0.70304	0.51307	18.859	15.561	38.388
Westdahl SAR-11	-1.4	68	1	0.70313	0.51304	18.867	15.563	38.403
Westdahl SAR-17	-1.4	27	1	0.70309	0.51304	18.870	15.562	38.398
repeat	-1.6	32	2					
Westdahl SAR-7	0.1	56	1	0.70313	0.51306	18.872	15.563	38.398
KR01-20	-2.0	43	1		0.51302	18.839	15.573	38.408
KRO1-6_11	0.5	41	1	0.70323	0.51304	18.791	15.557	38.341
repeat	0.7	45	2					
KR01-37_23	0.0	81	1	0.70349	0.51302	18.843	15.577	38.418
repeat	0.5	80	2					
KRO2-55_8	-2.0	115	1		0.51303	18.825	15.571	38.389
KR01-33_14	-2.3	165	1		0.51302	18.826	15.570	38.391
KR02-74_17	-0.9	194	1		0.51301	18.846	15.576	38.419
KR01-9_26	-2.3	244	1		0.51303	18.849	15.576	38.421
KR01-24_29	-2.1	297	1		0.51302	18.846	15.574	38.414

* - Radiogenic isotope data from (Kay, 1978; Sun, 1973)

Table 3

Table 3: Tl concentrations and isotopic compositions of Western Aleutian lavas

Sample	tn182_01_0 01	tn182_01_0 07	tn182_03_0 02	tn182_04_0 03	tn182_05_0 01	tn182_07_0 02	tn182_07_0 05	tn182_07_0 09	tn182_08_0 03	tn182_08_0 13	tn182_08_0 14	tn182_09_0 01	tn182_10_0 03	tn182_10_0 04	tn182_11_0 01	tn182_11_0 04	tn182_13_0 01	SO201-1b- 33-001	SO201-1b- 35-004	SO201-1b- 36-003
ultrasonic H2O																				
Eps 205 Tl	-3.2	-2.2	-2.2	-2.7	-2.6	-0.5	0.6	-2.7	-9.3	-2.3	-1.7	-1.5	-0.7	-3.4	-2.2	-2.0	-1.8	-3.1	-2.3	-1.3
Tl [ng/g]	110	59	54	65	54	69	23	151	476	69	66	83	124	298	123	79	94	56	48	33
Ultrasonic 1M HCl																				
Eps 205 Tl						-1.8	0.9		-9.2				0.6							
Tl [ng/g]						107	30		465				113							
Ultrasonic 6M HCl																				
Eps 205 Tl						-1.8	0.7	-2.5					-1.0							
Tl [ng/g]						106	30	184					160							
No treatment																				
Eps 205 Tl						0.3	2.2		-9.5				-0.6							
Tl [ng/g]						17	23		877				162							
1M HCl leach																				
Eps 205 Tl						9.8			0.3											
Tl [ng/g]						2			9											
Preferred Values																				
Eps 205 Tl	**-3.2**	**-2.2**	**-2.2**	**-2.7**	**-2.6**	**-1.8**	**0.7**	**-2.6**	**-9.3**	**-2.3**	**-1.7**	**-1.5**	**-0.4**	**-3.4**	**-2.2**	**-2.0**	**-1.8**	**-3.1**	**-2.3**	**-1.3**
Tl [ng/g]	**110**	**59**	**54**	**65**	**54**	**107**	**27**	**168**	**470**	**69**	**66**	**83**	**140**	**298**	**123**	**79**	**94**	**56**	**48**	**33**

Table 4

Table 4: Geochemical data for sediments outboard of the Aleutian arc

Site	Core	Section	Interval (cm)	Description	Eps 2IG Tl	87Sr/86Sr	143Nd/144Nd	206Pb/204Pb	207Pb/204Pb	208Pb/204Pb	Li	Be	Sc	V	Cr	Co	Ni	Cu	Ga	Zn	Rb	Sr	Y	Zr	Nb	Cs	Ba	La	Ce	Pr	Nd	Sm	Eu	Tb	Gd	Dy	Ho	Er	Yb	Lu	Hf	Ta	Tl	Pb	Th	U	ICP-ES:	SiO_2	Al_2O_3	MnO	Fe_2O_3	MgO	CaO	Na_2O	K_2O	P_2O_5
178	1	1	88-94	Silty clay	-2.6																																				0.42																		
178	12	2	112-117	Silty clay	-2.4																																				0.32																		
178	24	3	87-92	Silty clay/pebbles	-2.3																																				0.055																		
178	29	5	129-134	Silty clay	-1.6																																				0.058																		
repeat					-1.4																																				0.060																		
178	39	5	108-110	Volcanic ash	-1.5																																				0.261																		
178	47	1	127-130	Silt/v. fine sand	-2.2																																				0.41																		
178	47	1	141-145	Silt/v. fine sand	-2.5																																				0.62																		
178	57	1	136-140	Clay shale	-0.8																																				0.039																		
183	2R	3	52-54	Diatom rich silty clay	-1.8																																				0.28																		
183	9R	3	82-84	Clayey diatom ooze	-2.1																																				0.27																		
183	17R	3	72-74	Diatom ooze	-1.2																																				0.066																		
183	21R	1	129-131	Clay bearing diatom ooze	1.0																																				0.173																		
183	22R	2	95-97	Silty clay	2.0																																				0.55																		
183	24R	3	85-87	Clay	-3.1																																				0.42																		
183	27H	3	36-38	Silt	-2.6																																				0.34																		
183	27H	3	101-103	Clay	-2.6																																				0.39																		
183	31R	1	52-54	Silty sand	-2.5																																				0.30																		
183	38R	2	68-70	Clay	-2.9																																				0.40																		
183	39R	1	17-19	Silty clay	-2.9																																				0.36																		
183	39R	1	97-99	Limestone	-0.4																																				1.78																		
886C	1H	3	60-62	Reddish brown clay	0.6	0.71074	0.512138	18.740	15.636	38.811	40.6	2.62	25.2	116	50.0	49.6	59	187	59	115	95	198	21.5	121	9.85	8.55	2912	26.1	69.96	7.9	29.28	6.99	1.75	6.12	0.99	5.19	0.96	2.56	2.39	0.37	3.06	0.74	0.71	27.6	11.90	1.88		0.68	12.71	0.43	6.11	2.72	1.65	4.30	2.52	0.10
886C	1H	4	70-72	Reddish brown clay	0.9	0.71178	0.512311	18.727	15.640	38.830	41.7	2.36	19.6	95	48.3	42.5	68	166	57	106	93	160	16.2	105	9.42	9.01	2801	22.1	60.17	5.9	21.35	4.72	1.16	4.07	0.66	3.50	0.68	1.87	1.84	0.29	2.66	0.69	0.67	24.6	9.76	1.64		0.53	11.10	0.39	4.99	2.37	0.95	4.07	2.31	0.07
886C	2H	1	55-57	Dark brown spicule clay	-0.2																																																											
886C	2H	4	65-67	Light brown spicule clay	-1.7																																																									
886C	3H	1	90-92	Brown diatom clay	-1.2	0.71240	0.51229	18.726	15.643	38.853	42.7	3.00	24.0	91	51.2	60.0	108	225	110	123	109	197	17.4	142	11.65	10.27	5908	24.5	73.84	6.7	24.35	5.64	1.53	4.78	0.78	4.12	0.79	2.18	2.21	0.35	3.33	0.87	0.65	28.5	13.14	2.06		0.57	11.62	0.52	5.12	2.43	0.78	3.81	2.59	0.04
886C	3H	5	60-62	Light brown diatom ooze	-2.0																																																								
886C	4H	1	80-82	Light brown diatom ooze	-2.0						13.1	0.94	9.1	25	18.9	5.6	35	120	51	58	34	79	5.1	41	3.32	3.29	2995	8.2	24.18	2.3	7.78	1.86	0.49	1.52	0.24	1.25	0.23	0.63	0.65	0.10	0.90	0.23	0.170	7.0	4.07	0.59		0.16	3.43	0.03	1.54	1.09	0.30	3.47	0.84	0.01
886C	4H	5	30-32	Light brown diatom ooze	-1.7																																																							
886C	5H	1	50-52	Light brown diatom ooze	-0.5						21.7	1.60	14.3	53	15.1	21.2	175	232	44	266	41	127	11.7	105	3.87	3.33	2302	8.6	24.44	2.6	9.68	2.52	0.69	2.41	0.40	2.30	0.47	1.31	1.34	0.21	2.34	0.26	0.206	28.8	3.84	0.96		0.42	6.78	0.06	6.11	2.19	1.49	4.21	1.38	0.08
886C	5H	3	45-47	Light brown diatom ooze	-1.3																																																							
886C	6H	2	70-72	Light brown diatom ooze	-1.1																																																							
886C	6H	3	120-122	Mn nodule	10.9	0.70924	0.51246	18.606	15.630	38.739	12.4	5.28	13.3	62	10.2	2969	2234	3422	40	327	26	665	64.5	613	20.29	2.57	2497	154.5	1341.03	58.7	221.21	59.17	14.23	48.44	8.46	39.36	6.44	15.46	13.98	2.02	11.51	0.17	4.04	22.6	84.96	5.72		1.04	4.46	10.51	14.50	1.85	1.36	2.40	0.94	0.12
repeat					10.6																																																							
886C	7H	3	58-60	Dark brown clay	3.3				18.621	15.628	38.762	63.6	3.35	42.9	107	53.2	180.9	311	578	119	174	121	254	82.5	254	15.81	11.49	6216	55.7	195.51	20.5	82.35	22.43	5.77	21.11	3.46	18.61	3.54	9.45	9.14	1.47	6.32	1.06	1.62	48.9	21.16	3.15		0.72	15.57	1.66	6.65	3.08	1.18	3.31	3.49	0.29
repeat					3.7																																																						
886C	7H	5	73-75	Dark brown clay	-2.5				18.558	15.621	38.697																																																		
886C	8H	1	48-50	Dark brown clay	3.7	0.71003	0.51259	18.569	15.598	38.584	36.4	3.34	38.8	393	43.1	121.3	420	597	21	355	74	302	329.0	265	17.31	5.93	593	212.2	248.10	67.6	278.62	66.25	16.29	67.95	10.69	59.87	11.98	31.78	27.04	4.19	7.03	0.86	5.27	84.3	13.95	4.25		0.84	12.01	2.73	15.53	3.02	3.44	2.74	2.91	2.34
repeat								18.570	15.598	38.587																																																	
886C	8H	4	58-60	Dark brown clay	6.4				18.416	15.522	38.002	21.8	6.34	22.5	846	14.5	72.7	685	1211	25	850	28	492	373.3	271	9.68	2.22	1394	359.5	93.01	113.7	462.77	106.55	25.68	103.40	15.99	85.62	16.34	41.45	33.56	4.89	4.82	0.36	20.67	146.3	4.07	6.24		0.34	5.91	8.24	35.45	2.39	2.20	2.24	1.34	1.77
886B	9X	1	60-62	Highly altered basalt, breccia	-2.7			19.082	15.627	38.367	23.9	0.99	30.2	171	61.1	59.7	180	148	12	191	26	177	19.9	83	1.02	0.70	48	8.9	8.02	2.9	12.49	3.63	1.38	4.59	0.80	4.80	0.94	2.44	2.06	0.30	2.25	0.89	1.12	2.01	0.068	0.98		1.31	21.17	0.17	11.55	1.71	0.57	2.76	2.95	0.20

Trace element and radiogenic isotope data from DSDP 178 and DSDP 183 from Plank & Langmuir (1998) and Kay & Kay (1988)

Figure 1

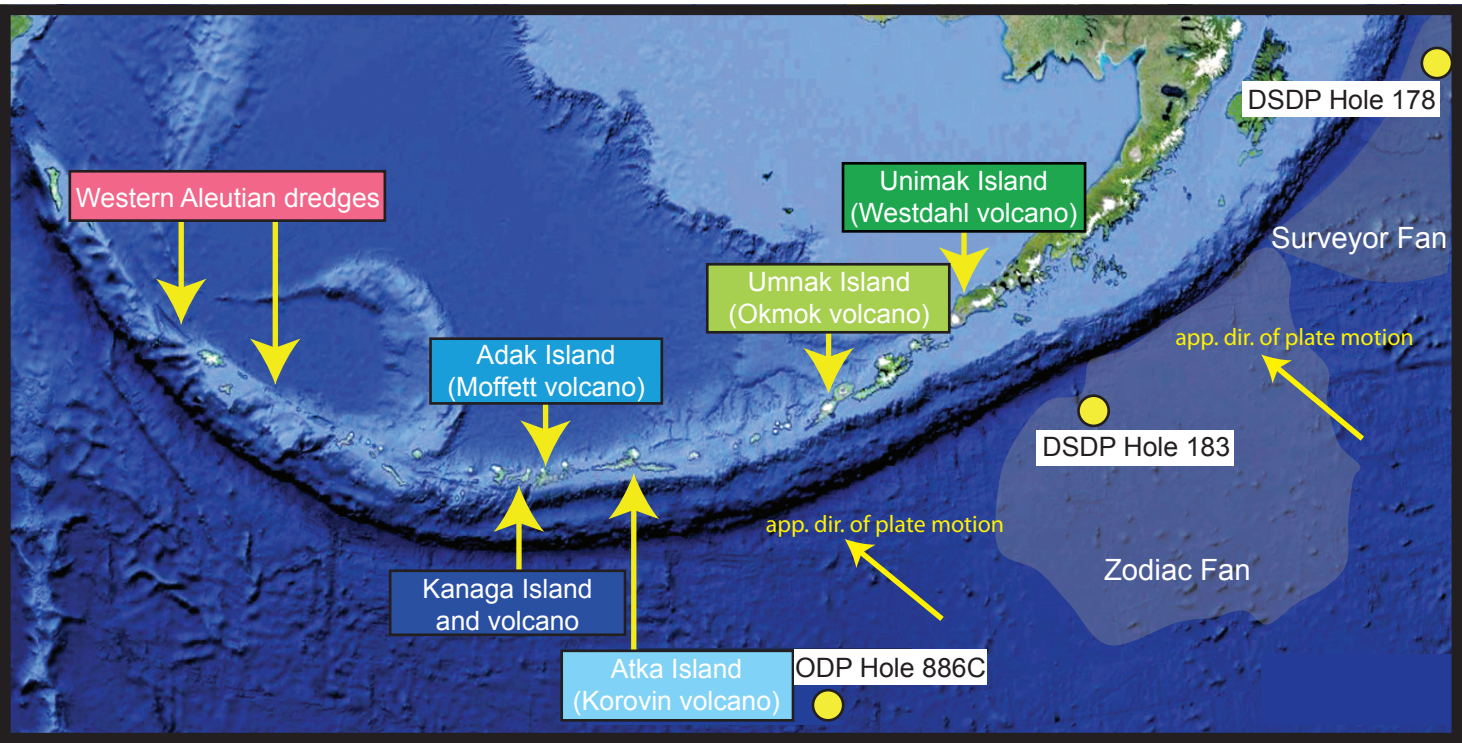
DSDP Hole 178
Western Aleutian dredges
Unimak Island
(Westdahl volcano)
Surveyor Fan
Umnak Island
(Okmok volcano)
app. dir. of plate motion
Adak Island
(Moffett volcano)
DSDP Hole 183
app. dir. of plate motion
Zodiac Fan
Kanaga Island
and volcano
Atka Island
(Korovin volcano)
ODP Hole 886C

Figure 2

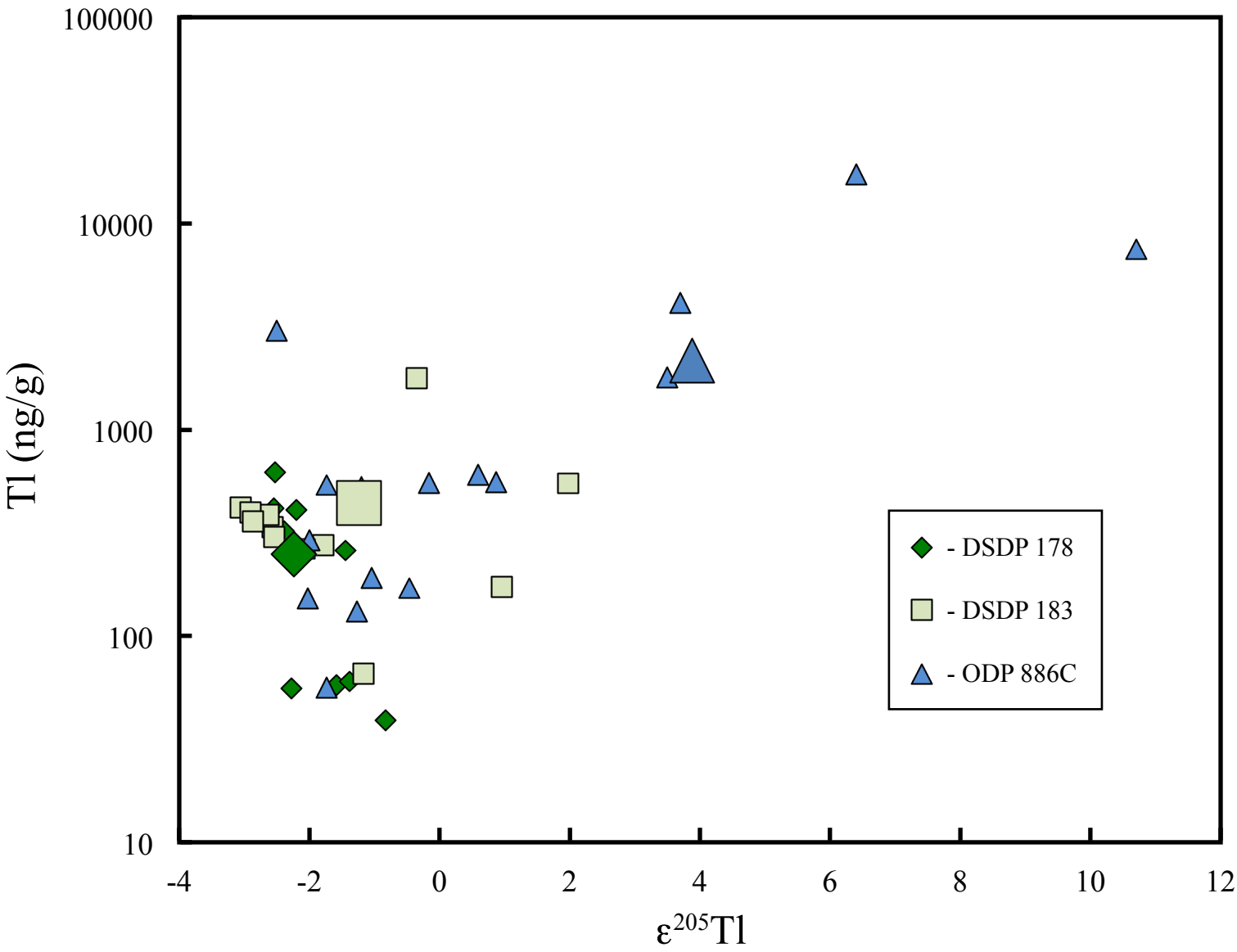
100000
10000
1000
100
10
Tl (ng/g)
-4
-2
0
2
4
6
8
10
12
ε205Tl
- DSDP 178
- DSDP 183
- ODP 886C

Figure 3

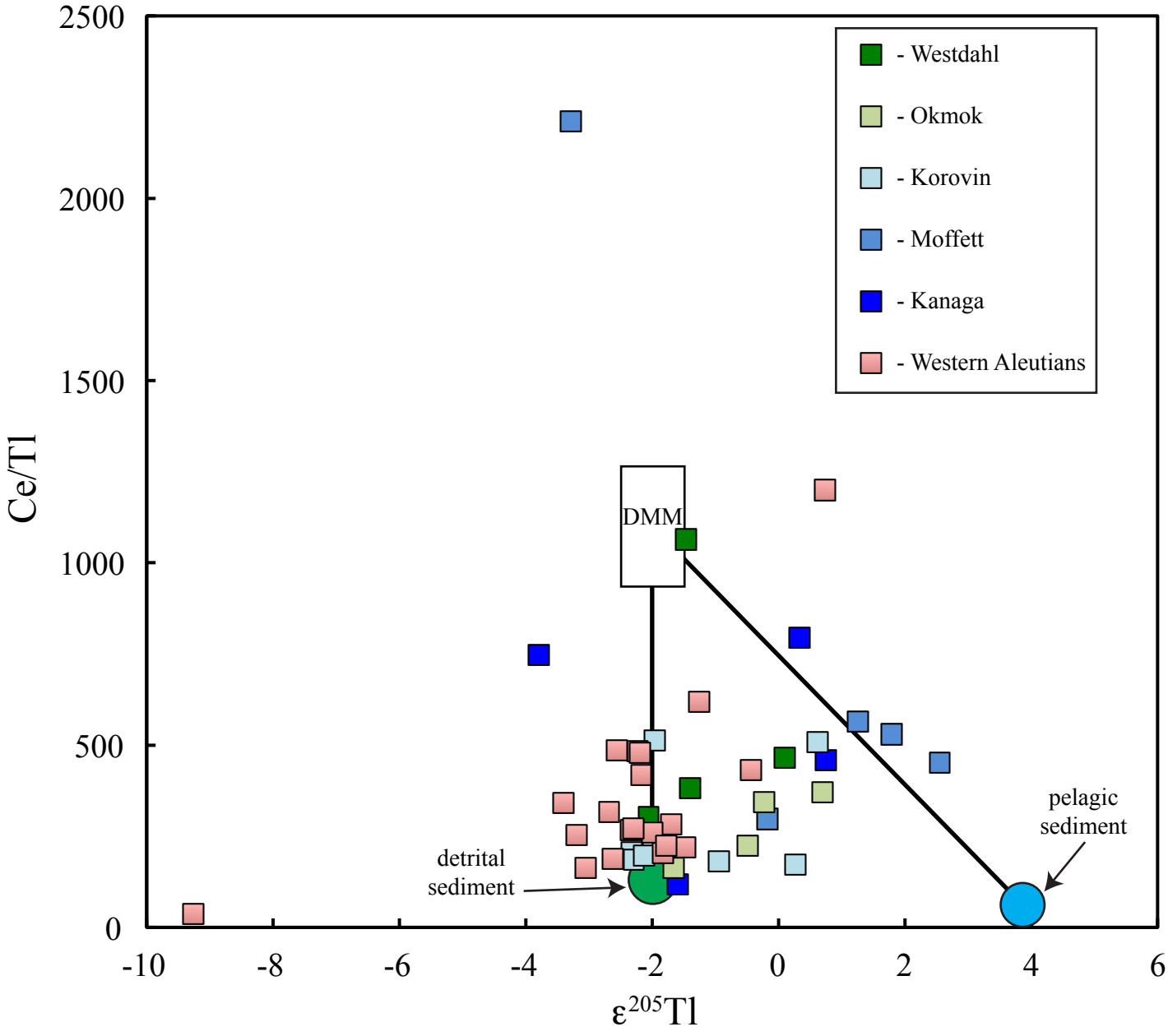
Figure 3
2500
2000
1500
1000
500
0
Ce/Tl
-10
-8
-6
-4
-2
0
2
4
6
ε205Tl
- Westdahl
- Okmok
- Korovin
- Moffett
- Kanaga
- Western Aleutians
DMM
detrital sediment
pelagic sediment

Figure 4

Figure 4

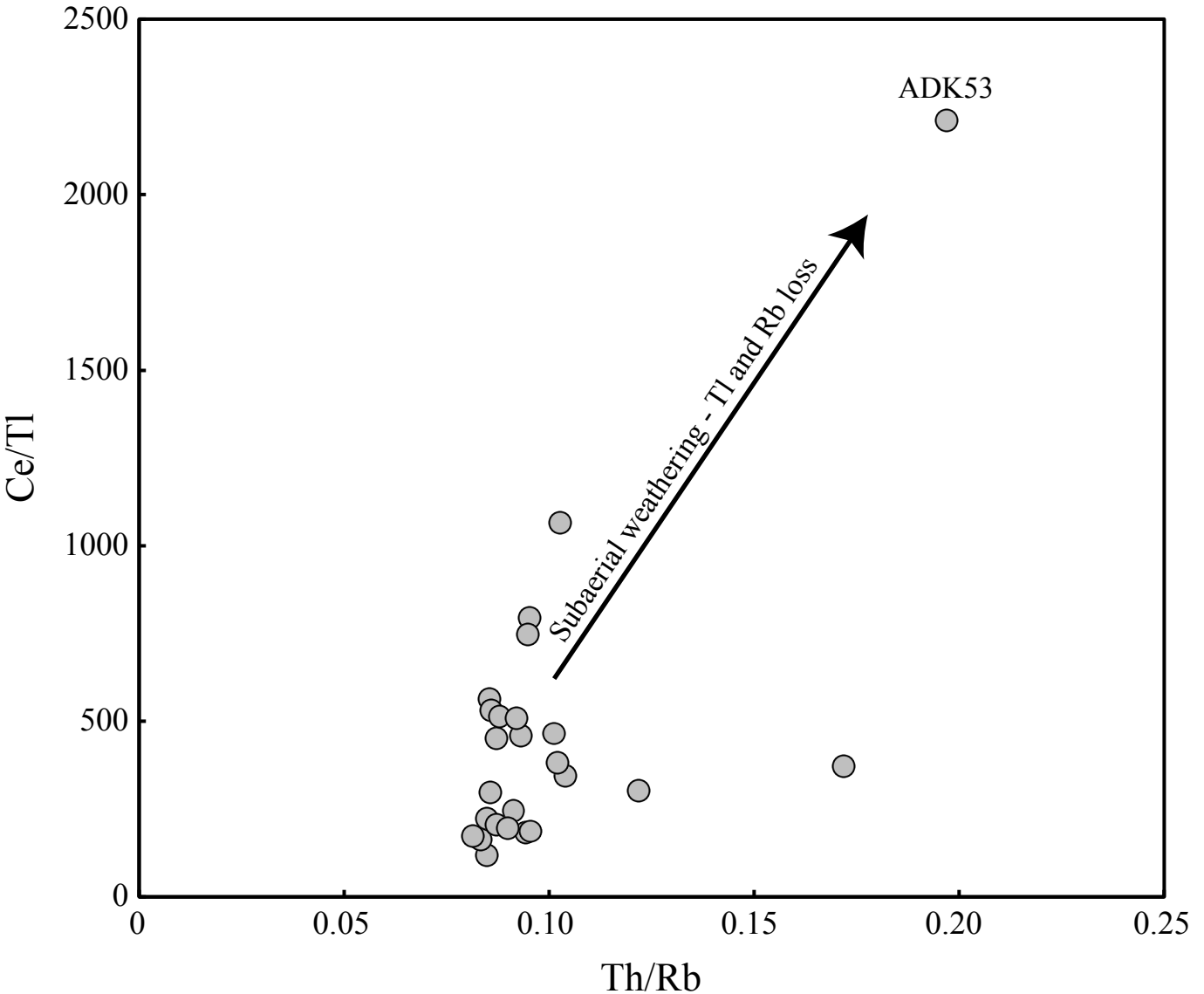

Figure 5

Figure 5

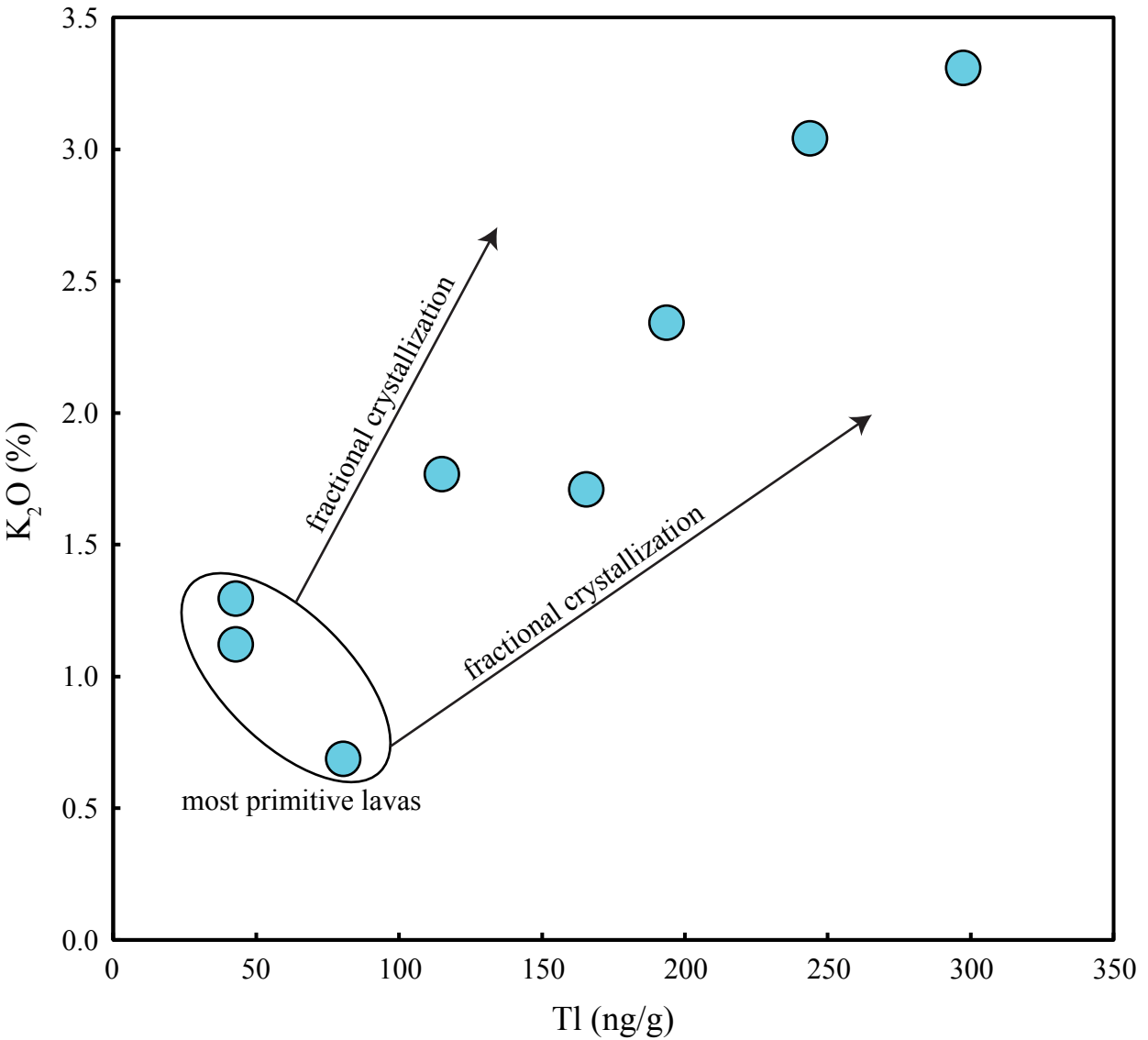

Figure 6

Figure 6

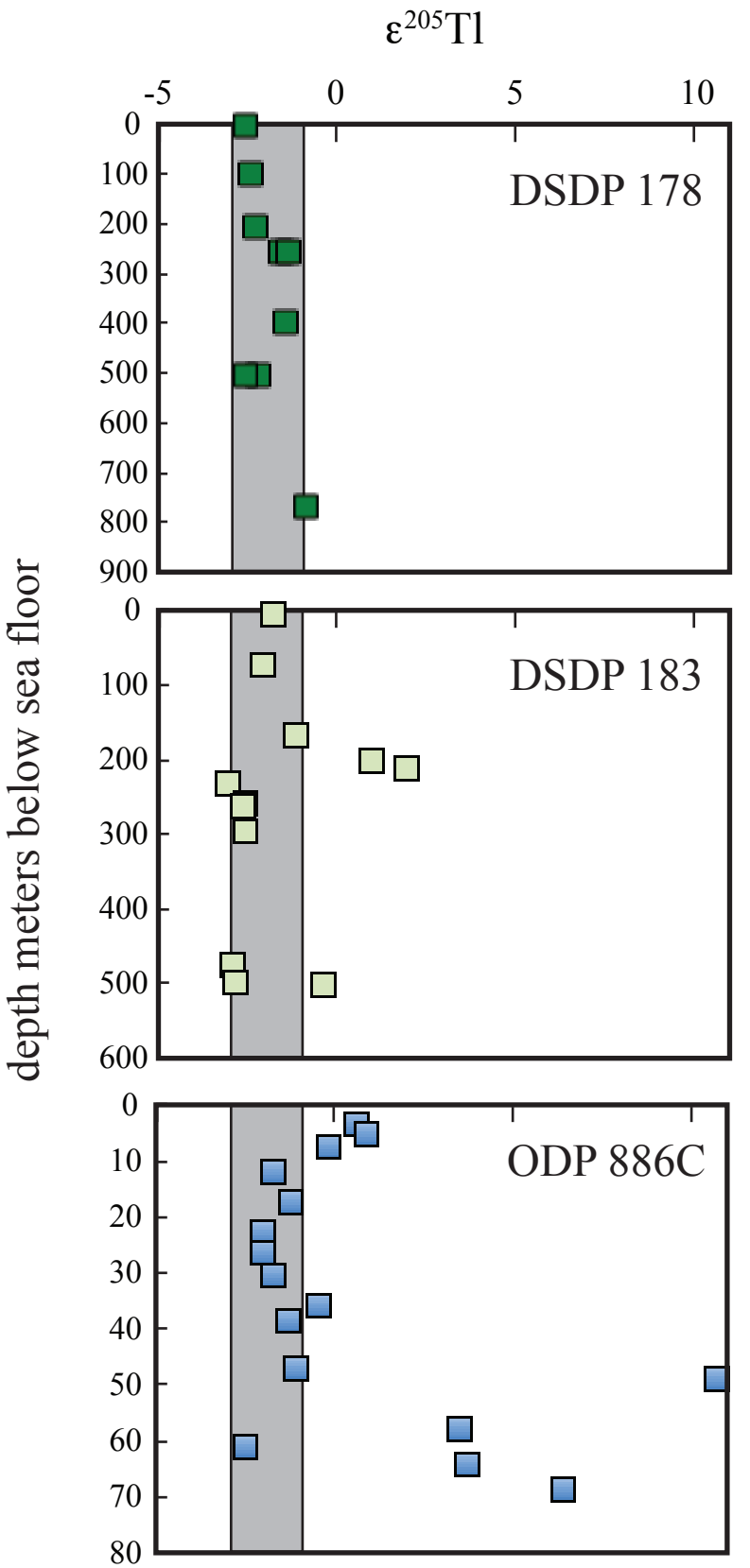

Figure 7

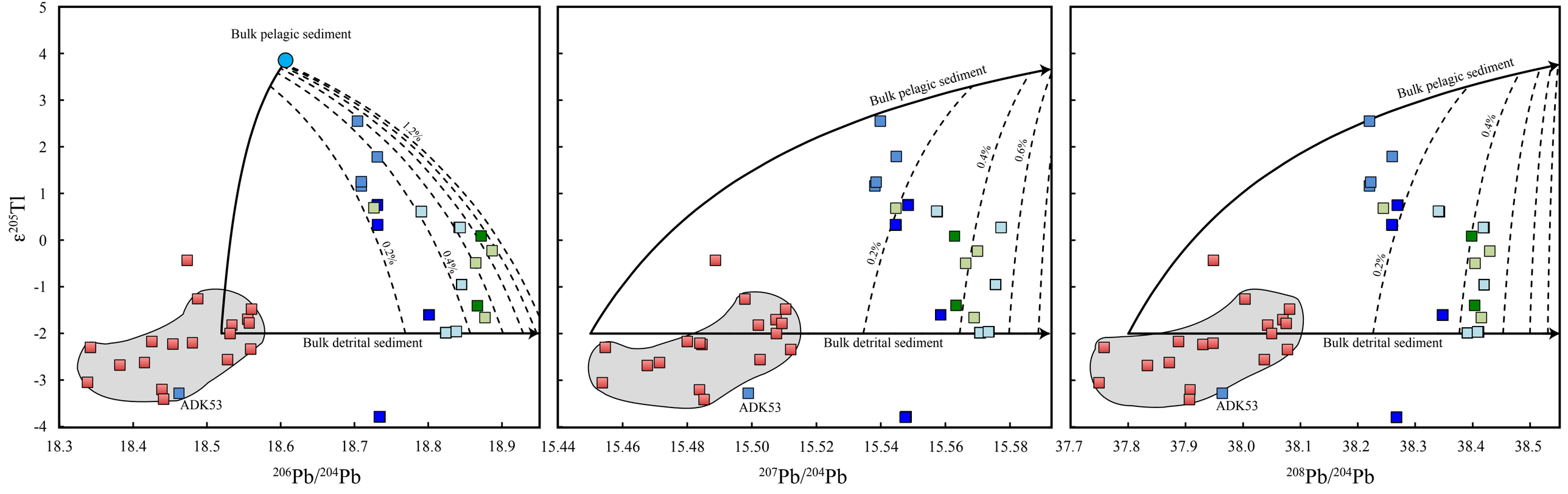
Figure 7
Bulk pelagic sediment
Bulk detrital sediment
ADK53
1.2%
0.2%
0.4%
0.6%
ε205Tl
206Pb/204Pb
207Pb/204Pb
208Pb/204Pb

Figure 8

Figure 8

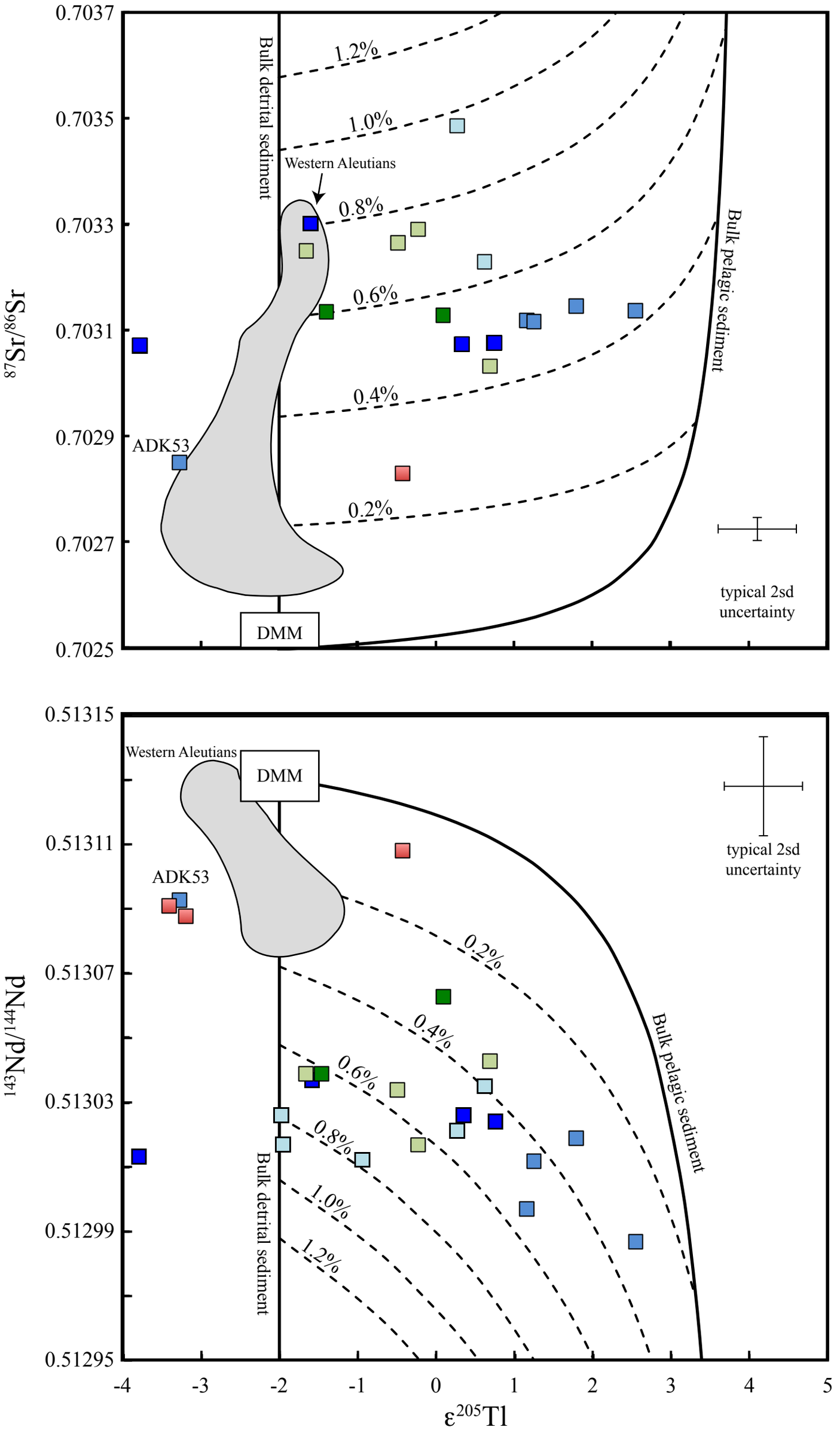

Figure 9

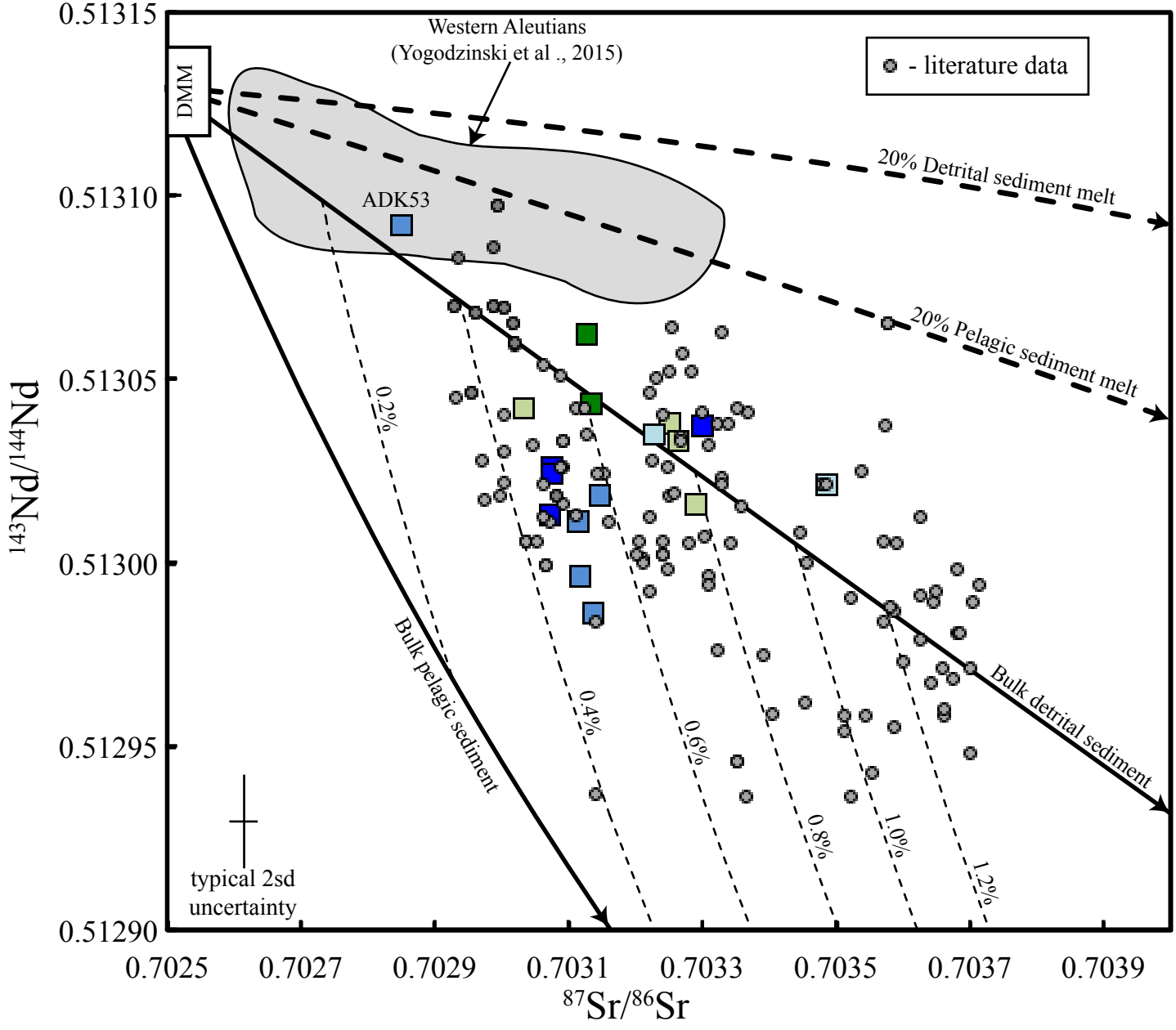
0.51315
0.51310
0.51305
0.51300
0.51295
0.51290
$^{143}Nd/^{144}Nd$
0.7025
0.7027
0.7029
0.7031
0.7033
0.7035
0.7037
0.7039
$^{87}Sr/^{86}Sr$
DMM
Western Aleutians
(Yogodzinski et al ., 2015)
ADK53
- literature data
20% Detrital sediment melt
20% Pelagic sediment melt
0.2%
0.4%
0.6%
0.8%
1.0%
1.2%
Bulk pelagic sediment
Bulk detrital sediment
typical 2sd
uncertainty

Figure 10

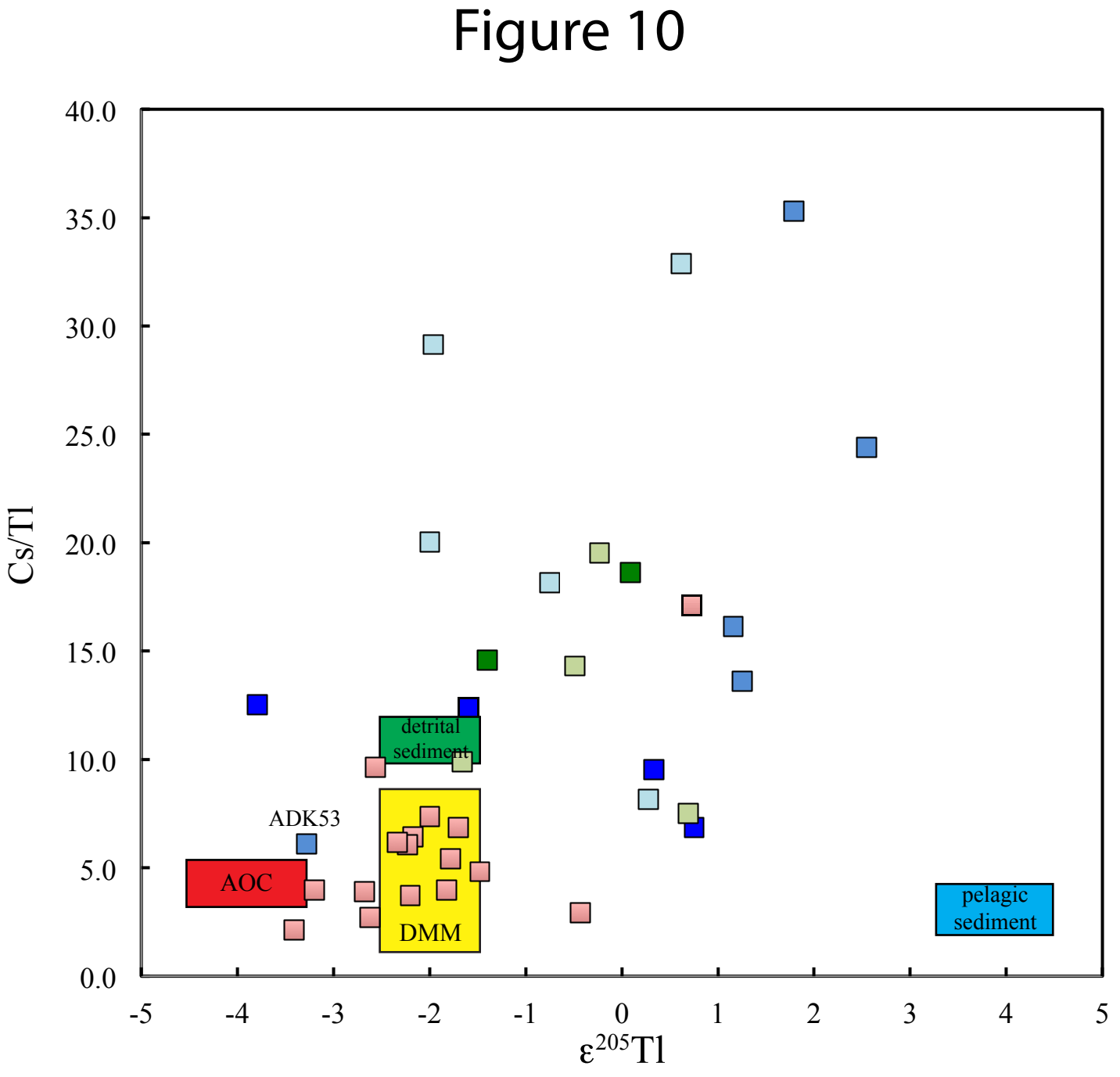
Figure 10
40.0
35.0
30.0
25.0
20.0
15.0
10.0
5.0
0.0
Cs/Tl
-5
-4
-3
-2
-1
0
1
2
3
4
5
ε205Tl
detrital sediment
ADK53
AOC
DMM
pelagic sediment